

Scale-invariant scale-channel networks: Deep networks that generalise to previously unseen scales

Ylva Jansson and Tony Lindeberg

Abstract The ability to handle large scale variations is crucial for many real world visual tasks. A straightforward approach for handling scale in a deep network is to process an image at several scales simultaneously in a set of *scale channels*. Scale invariance can then, in principle, be achieved by using weight sharing between the scale channels together with max or average pooling over the outputs from the scale channels. The ability of such *scale channel networks* to generalise to scales not present in the training set over significant scale ranges has, however, not previously been explored.

In this paper, we present a systematic study of this methodology by implementing different types of scale channel networks and evaluating their ability to generalise to previously unseen scales. We develop a formalism for analysing the covariance and invariance properties of scale channel networks, and explore how different design choices, unique to scaling transformations, affect the overall performance of scale channel networks. We first show that two previously proposed scale channel network designs do not generalise well to scales not present in the training set. We explain theoretically and demonstrate experimentally why generalisation fails in these cases. We then propose a new type of *foveated scale channel architecture*, where the scale channels process increasingly larger parts of the image with decreasing resolution. This new type of scale channel network is shown to generalise extremely well, provided sufficient image resolution and the absence of boundary effects. Our proposed FovMax and FovAvg networks perform almost identically over a scale range of 8, also when training on *single scale training data*, and do also give improved performance

The support from the Swedish Research Council (contract 2018-03586) is gratefully acknowledged.

Computational Brain Science Lab, Division of Computational Science and Technology, KTH Royal Institute of Technology, SE-100 44 Stockholm, Sweden. E-mail: yjansson@kth.se · tony@kth.se

when learning from datasets with large scale variations in the small sample regime.

Keywords Deep learning · Convolutional neural networks · Invariant neural networks · Scale covariance · Scale invariance · Scale generalisation · Scale space

1 Introduction

Scaling transformations are as pervasive in natural image data as translations. In any natural scene, the size of the projection of an object on the retina or a digital sensor varies continuously with the distance between the object and the observer. Compared to translations, scale variability is in some sense harder to handle for a biological or artificial agent. It is possible to fixate an object, thus centering it on the retina. The equivalence for scaling, which would be to ensure a constant distance to objects before further processing, is not a viable solution. A human observer can nonetheless recognise an object at a range of scales, from a single observation, and there is, indeed, experimental evidence demonstrating scale invariant processing in the primate visual cortex [1, 2, 3, 4, 5, 6]. Convolutional neural networks (CNNs) already encode structural assumptions about translation invariance and locality, which by the successful application of CNNs for computer vision tasks has been demonstrated to constitute useful priors for processing visual data. We propose that structural assumptions about scale, could similarly to translation covariance, be a useful prior in convolutional neural networks.

Encoding structural priors about a larger group of visual transformations, including scaling transformations and affine transformations, is an integrated part of a range of successful classical computer vision approaches [7, 8, 9, 10, 11, 12, 13, 14, 15, 16, 17, 18] and in a theory for explaining the computational function of early visual receptive fields

[19,20]. There is also a growing body of work on invariant CNNs, especially concerning invariance to 2D/3D rotations and flips [21,22,23,24,25,26,27,28,29,30,31,32,33,34,35,36]. There has been some work done on scale invariant recognition in CNNs, where recent approaches [37,38,39,40,41] have shown improvements compared to standard CNNs for scale variability present both in the training and the testing sets. These approaches have, however, either not been evaluated for the task of generalisation to scales *not present in the training set* [38,42,39,41] or only across a very limited scale range [37,40]. Thus, the possibilities for CNNs to generalise to previously unseen scales have, however, so far not been well explored.

The structure of a standard CNN implies a preferred scale as decided by the fixed size of the filters (often 3×3 or 5×5 kernels) together with the depth and max-pooling strategy applied. This determines the resolution at which the image is processed and the size of the receptive fields of individual units at different depths. A vanilla CNN is, therefore, not designed for multi-scale processing. Because of this, state-of-the-art object detection approaches (where the scale variability is significantly larger compared to classification) employ different mechanisms, such as branching off classifiers at different depths [43,44], learning to transform the input or the filters [45,46,47], or by combining the deep network with different types of image pyramids [48,49,50,51,52,53].

The goal of these approaches has, however, not been to *generalise between scales* and even though they enable multi-scale processing, they lack the type of structure necessary for true scale invariance. Thus, it is not possible to predict how they will react to objects appearing at new scales in the testing set or a to real world scenario. This can lead to undesirable effects as shown in the rich literature on adversarial examples, where it has been demonstrated that CNNs suffer from unintuitive failure modes when presented with data outside the training distribution [54,55,56,57,58,59,60]. This includes adversarial examples constructed by means of small translations, rotations and scalings [61,62], that is transformations that are partially represented in a training set of natural images. *Scale-invariant CNNs* could enable both multi-scale processing and predictable behaviour when encountering objects at novel scales, without the need to fully span all possible scales in the training set.

Most likely, a set of different strategies will be needed to handle the full scale variability in the natural world. *Full invariance* over scale factors of 100 or more as present in natural images might not be viable in a network with similar type of processing at fine and coarse scales¹. We argue, however,

¹ When analysing image data with very large scale variations, the finite receptive field of any detector and the difference in image resolution between objects observed at different scales will imply a large difference in appearance between very small and very large objects.

that a deep learning based approach that is invariant over a significant scale range could be an important part of the solution to handling also such large scale variations. Note, that the term *scale invariance* has sometimes, in the computer vision literature, been used in a weaker sense of "the ability to process objects of varying sizes" or "learn in the presence of scale variability". We will here use the term in a stricter classical sense of a classifier/feature extractor whose output does not change when the input is transformed.

One of the simplest CNN architectures used for covariant and invariant image processing is a channel network (also referred to as siamese network) [63,26,64]. In such an architecture, transformed copies of the input image are processed in parallel by different "channels" (subnetworks) corresponding to a set of image transformations. This approach can together with weight sharing and max or average pooling over the output from the channels enable invariant recognition for finite transformation groups, such as 90 degree rotations and flips. An *invariant scale channel network* is a natural extension of invariant channel networks as previously explored for rotations in [26]. It can equivalently be seen as a way of extending ideas underlying the classical scale-space methodology to deep learning [65,66,67,68,69,70,71,72,73,74,75], in the sense that the in the absense of further information, the image data is processed at all scales simultaneously, and that the outputs from the scale channels will constitute a non-linear scale-covariant multi-scale representation of the input image.

1.1 Contribution and novelty

The subject of this paper is to investigate the possibility to construct a scale invariant CNN based on a scale channel architecture. The key contributions of our work are to implement different possible types of scale channel networks and to evaluate the ability of these networks to generalise to previously unseen scales, so that we can train a network at some scale(s) and test it at other scales, without complementary use of data augmentation. It should be noted that previous scale channel networks exist, but those are explicitly designed for multi-scale processing [76,77] rather than scale invariance or have not been evaluated with regard to their ability to generalise to unseen scales over any significant scale range [37]. We here implement and evaluate networks based on principles similar to these previous approaches but also a new type of foveated scale channel network, where the individual scale channels process increasingly larger parts of the image with decreasing resolution.

This implies that fully invariant processing over such wide scale ranges might not be an applicable strategy. Instead different strategies will likely be needed to recognise objects at very low resolution from those needed to recognise objects at very high resolutions.

To enable testing each approach over a large range of scales, we create a new variation of the MNIST dataset, referred to as MNIST Large Scale, with scale variations up to a factor of 8. This represents a dataset with sufficient resolution and image size to enable invariant recognition over a large range of scale factors. We also rescale the CIFAR-10 dataset over a scale factor of 4, which is a wider scale range than has previously been evaluated for this dataset. This rescaled CIFAR-10 dataset is used to test if scale-invariant networks can still give significant improvements in generalisation to new scales, in the presence of limited image resolution and for small image sizes. We evaluate the ability to generalise to previously unseen scales for the different types of channel networks by first training on a single scale or a limited range of scales and then testing recognition for scales not present in the training set. The results are compared a standard CNN baseline.

Our experiments on the MNIST Large Scale dataset show that two previously used scale channel network designs or methodologies do, in fact, not generalise well to scales not present in the training set. The first type of method is based on *concatenating the outputs from the scale channels* and using this as input to a fully connected layer (as opposed to applying max or average pooling over the scale-dimension). We show that such a network does not learn to combine the output from the scales channels in a correct way as to enable generalisation to previously unseen scales. The reason for this is the absence of a structure to enforce invariance. The second type of method is to handle the difference in image size between rescaled images, by applying the subnetwork corresponding to each channel in a *sliding window manner*. This methodology, however, implies that the rescaled copies of an image are not processed *in the same way*, since for an object processed in scale channels corresponding to an up-scaled image, a large range of different, (e.g. non-centered) object views, will be processed, compared to only processing the central view for an object in a down-scaled image. This implies that invariance cannot be achieved, since max (or average) pooling will be performed over *different views of the objects for different scales*, which implies that the max (or average) over the scale dimension is not be guaranteed to be stable when the input is transformed.

We do, instead, propose a new type of foveated scale channel architecture, where the scale channels process increasingly larger parts of the image with decreasing resolution. Together with max and average pooling, this leads to our FovMax and FovAvg networks. We show that this approach enables extremely good generalisation when the image resolution is sufficient and there is an absence of boundary effects. Notably, for rescalings of MNIST, almost identical performance over a scale range of 8 is achieved, when training on *single size* training data. We further show that, also on the CIFAR-10 dataset, in the presence of severe limita-

tions regarding image resolution and image size, the foveated scale channel networks still provide considerably better generalisation ability compared to both a standard CNN and alternative scale channel approaches. We also demonstrate that the FovMax and FovAvg networks give improved performance for datasets with large scale variations in both the training and testing data, in the small sample regime.

We propose that the presented foveated scale channel networks will prove useful in situations where a simple approach that can generalise to unseen scales or learning from small datasets with large scale variations is needed. Our study also highlights possibilities and limitations for scale invariant CNNs and provides a simple baseline to evaluate other approaches against. Finally, we see possibilities to integrate the foveated scale channel network, or similar types of foveated scale invariant processing, as subparts in more complex frameworks dealing with large scale variations.

1.2 Relations to previous contribution

This paper constitutes a substantially extended version of a conference paper presented at the ICPR 2020 conference [78] and with substantial additions concerning:

- the motivations underlying this work and the importance of a scale generalisation ability for deep networks (Section 1),
- a wider overview of related work (Section 1 and Section 2),
- theoretical relationships between the presented scale channel networks and the notion of scale-space representation (Section 3.6 and Appendix A),
- theoretical relationships between the presented scale channel networks and scale-normalised derivatives with associated methods for scale selection (Section 3.6 and Appendix B),
- more extensive experimental results on the MNISTLarge-Scale dataset, specifically new experiments that investigate (i) the dependency on the scale range spanned by the scale channels, (ii) the dependency on the sampling density of the scale levels in the scale channels, (iii) the influence of multi-scale learning over different scale intervals, and (iv) an analysis of the scale selection properties over the multiple scale channels for the different types of scale channel networks (Section 5),
- experimental results for the CIFAR-10 dataset subject to scaling transformations of the testing data (Section 6),
- details about the dataset creation for the MNIST Large Scale dataset (Appendix C).

In relation to the ICPR 2020 paper, this paper therefore gives a more general motivation for scale channel networks in relation to the topic of scale generalisation, presents more experimental results for further use cases and additional datasets,

gives deeper theoretical relationships between scale channel networks and scale-space theory and gives overall better descriptions of several of the subjects treated in the paper, including more extensive references to related literature.

2 Relations to previous work

In the area of scale-space theory [65, 66, 67, 68, 69, 70, 71, 72, 73, 74, 75], a multi-scale representation of an input image is created by convolving the image with a set of rescaled Gaussian kernels and Gaussian derivative filters, which are then often combined in non-linear ways. In this way, a powerful methodology has been developed to handle scaling transformations in classical computer vision [7, 8, 9, 10, 11, 13, 14, 15, 16, 18]. The scale channel networks described in this paper can be seen as an extension of this philosophy of processing an image *at all scales simultaneously* as a means of achieving scale invariance, but instead using deep non-linear feature extractors learned from data, as opposed to hand-crafted image features and image descriptors.

CNNs can give impressive performance, but they are sensitive to scale variations. Provided that the architecture of the deep network is sufficiently flexible, moderate increase in the robustness to scaling transformations can be obtained by augmenting the training images with multiple rescaled copies of each training image (scale jittering) [79, 80]. The performance does, however, degrade for scales not present in the training set [81, 62, 82], and different network structure may be optimal for small *vs.* large images [82]. It is furthermore possible to construct adversarial examples by means of small translations rotations and scalings [61, 62].

State-of-the-art CNN based object detection approaches all employ different mechanisms to deal with scale variability, *e.g.*, branching off classifiers at different depths [44], learning to transform the input or the filters [45, 46, 47], or using different types of image pyramids [48, 49, 50, 51, 52, 53], or other approaches, where the image is rescaled to different resolutions, possibly combined with interactions or pooling between the layers [83, 84, 85, 82]. There are also deep networks that somehow handle the notion of scale by approaches, such as dilated convolutions [86, 87, 88], scale-dependent pooling [89], scale-adaptive convolutions [90], by spatially warping the image data by a log-polar transformation prior to image filtering [47, 42], or adding additional branches of down-samplings and/or up-samplings in each layer of the network [91, 92]. The goal of these approaches has, however, not been to generalise to *previously unseen scales* and they lack the structure necessary for true scale invariance.

Examples of handcrafted scale invariant hierarchical descriptors are [93, 94]. We are, here, interested in combining scale invariance with learning. There exist some previous work aimed explicitly at scale invariant recognition in CNNs

[37, 38, 39, 40, 41]. These approaches have, however, either not been evaluated for the task of generalisation to scales *not present in the training set* [38, 39, 41] or only across a very limited scale range [37, 40]. Previous scale channel networks exist, but are explicitly designed for multi-scale processing [76, 77] rather than scale invariance, or have not been evaluated with regard to their ability to generalise to unseen scales over any significant scale range [48, 37]. A dual approach to scale channel networks, that, however, allows for scale invariance and scale generalisation, is presented in [95], based on transforming continuous CNNs expressed in terms of continuous functions for the filter weights with respect to scaling transformations.

There is a large literature on approaches to achieve rotation-covariant networks [25, 26, 27, 28, 29, 30, 31, 32, 33, 34] with applications to different domains, including astronomy [64], remote sensing [96], medical image analysis [97, 98, 99] and texture classification [100]. There are also approaches to invariant networks based on formalism from group theory [24, 101, 102].

3 Theory of continuous scale channel networks

In this section, we will introduce a mathematical framework for modelling and analysing scale channel networks based on a continuous model of the image space. This model enables straightforward analysis of the covariance and invariance properties of the channel networks, that are later approximated in a discrete implementation. We, here, generalise previous analysis of invariance properties of channel networks [26] to scale channel networks. We further analyse covariance properties and additional options for aggregating information across transformation channels.

3.1 Images and image transformations

We consider images $f : \mathbb{R}^N \rightarrow \mathbb{R}$ that are measurable functions in $L_\infty(\mathbb{R}^N)$ and denote this space of images as V . A *group of image transformations* corresponding to a group G is a family of image transformations \mathcal{T}_g ($g \in G$) with a group structure, *i.e.*, fulfilling the group axioms of closure, identity, associativity and inverse. We denote the combination of two group elements $g, h \in G$ by gh and the cardinality of G as $|G|$. Formally, a group G induces an *action on functions* by acting on the underlying space on which the function is defined (here the image domain). We are here interested in the group of *uniform scalings* around x_0 with the group action

$$(\mathcal{S}_{s, x_0} f)(x') = f(x), \quad x' = S_s(x - x_0) + x_0, \quad (1)$$

where $S_s = \text{diag}(s)$. For simplicity, we often assume $x_0 = 0$ and denote $\mathcal{S}_{s,0}$ as \mathcal{S}_s corresponding to

$$(\mathcal{S}_s f)(x) = f(S_s^{-1}x) = f_s(x). \quad (2)$$

We will also consider the translation group with the action (where $\delta \in \mathbb{R}^N$)

$$(\mathcal{D}_\delta f)(x') = f(x), \quad x' = x + \delta. \quad (3)$$

3.2 Invariance and covariance

Consider a general feature extractor $\Lambda : V \rightarrow \mathbb{K}$ that maps an image $f \in V$ to a feature representation $y \in \mathbb{K}$. In our continuous model, \mathbb{K} will typically correspond to a set of M feature maps (functions) so that $\Lambda f \in V^M$. This is a continuous analogue of a discrete convolutional feature map with M features.

A feature extractor² Λ is *covariant* to a transformation group G (formally to the group action) if there exists an *input independent* transformation $\tilde{\mathcal{T}}_g$ that can align the feature maps of a transformed image with those of the original image

$$\Lambda(\mathcal{T}_g f) = \tilde{\mathcal{T}}_g(\Lambda f) \quad (4)$$

for all $g \in G$ and $f \in V$. Thus, for a covariant feature extractor it is possible to predict the feature maps of a transformed image from the feature maps of the original image, as visualised in the commutative diagram in Figure 1.

$$\begin{array}{ccc} \Lambda f & \xrightarrow{\tilde{\mathcal{T}}_g} & \Lambda(\mathcal{T}_g f) = \tilde{\mathcal{T}}_g(\Lambda f) \\ \uparrow \Lambda & & \uparrow \Lambda \\ f & \xrightarrow{\mathcal{T}_g} & \mathcal{T}_g f \end{array}$$

Fig. 1: Commutative diagram for a covariant feature extractor Λ with its associated possibly transformed feature extractor Λ' , under the action of a transformation \mathcal{T}_g with its associated possibly transformed transformation $\tilde{\mathcal{T}}_g$.

A feature extractor Λ is *invariant* to a transformation group G if the feature representation of a transformed image is *equal to* the feature representation of the original image

$$\Lambda(\mathcal{T}_g f) = \Lambda(f) \quad (5)$$

for all $g \in G$ and $f \in V$. Invariance is thus a special case of covariance where $\tilde{\mathcal{T}}_g$ is the identity transformation.

² With regard to the scale channel networks that we develop later in this paper, a *covariant* feature extractor Λ should be seen as representing the entire family of scale channels, as the union of all the scale channels, not a single scale channel in isolation. An *invariant* feature extractor Λ will on the other hand correspond to the result of max pooling or average pooling over all the scale channels.

3.3 Continuous model of a CNN

Let $\phi : V \rightarrow V^{M_k}$ denote a continuous CNN with k layers and M_i feature channels in layer i . Let $\theta^{(i)}$ represent the transformation between layers $i-1$ and i such that

$$(\phi^{(i)} f)(x, c) = (\theta^{(i)} \theta^{(i-1)} \dots \theta^{(2)} \theta^{(1)} f)(x, c), \quad (6)$$

where $c \in \{1, 2, \dots, M_k\}$ denotes the feature channel and $\phi = \phi^{(k)}$. We model the transformation $\theta^{(i)}$ between two adjacent layers $\phi^{(i-1)} f$ and $\phi^{(i)} f$ as a convolution followed by the addition of a bias term $b_{i,c} \in \mathbb{R}$ and the application of a pointwise non-linearity $\sigma_i : \mathbb{R} \rightarrow \mathbb{R}$:

$$\begin{aligned} & (\phi^{(i)} f)(x, c) \\ &= \sigma_i \left(\sum_{m=1}^{M_{i-1}} \int_{\xi \in \mathbb{R}^N} (\phi^{(i-1)} f)(x - \xi, m) g_{m,c}^{(i)}(\xi) d\xi + b_{i,c} \right) \end{aligned} \quad (7)$$

where $g_{m,c}^{(i)} \in L_1(\mathbb{R}^N)$ denotes the convolution kernel that propagates information from feature channel m in layer $i-1$ to output feature channel c in layer i . A final fully connected classification layer with compact support can also be modelled as a convolution combined with a non-linearity σ_k that represents a *softmax operation* over the feature channels.

3.4 Scale channel networks

The key idea underlying *channel networks* is to process transformed copies of an input image in parallel, in a set of network “channels” (subnetworks) with shared weights. For finite transformation groups, such as discrete rotations, using one channel corresponding to each group element and applying max pooling over the channel dimension can give an invariant output code. For continuous but compact groups, invariance can instead be achieved for a discrete subgroup.

The scaling group does, however, imply additional challenges, since it is neither finite nor compact. The key question that we address here, is whether a scale channel network can still support invariant recognition.

We will define a multi-column *scale channel network* $\Lambda : V \rightarrow V^{M_k}$ for the group of scaling transformations S by using a single base network $\phi : V \rightarrow V^{M_k}$ to define a set of *scale channels* $\{\phi_s\}_{s \in S}$

$$(\phi_s f)(x, c) = (\phi \mathcal{S}_s f)(x, c) = (\phi f_s)(x, c), \quad (8)$$

where each channel thus applies exactly the same operation to a scaled copy of the input image (see Figure 2(a)). We will denote the mapping from the input image to the scale channel feature maps at depth i as $\Gamma^{(i)} : V \rightarrow V^{M_i |S|}$

$$(\Gamma^{(i)} f)(x, c, s) = (\phi_s^{(i)} f)(x, c) = (\phi^{(i)} \mathcal{S}_s f)(x, c). \quad (9)$$

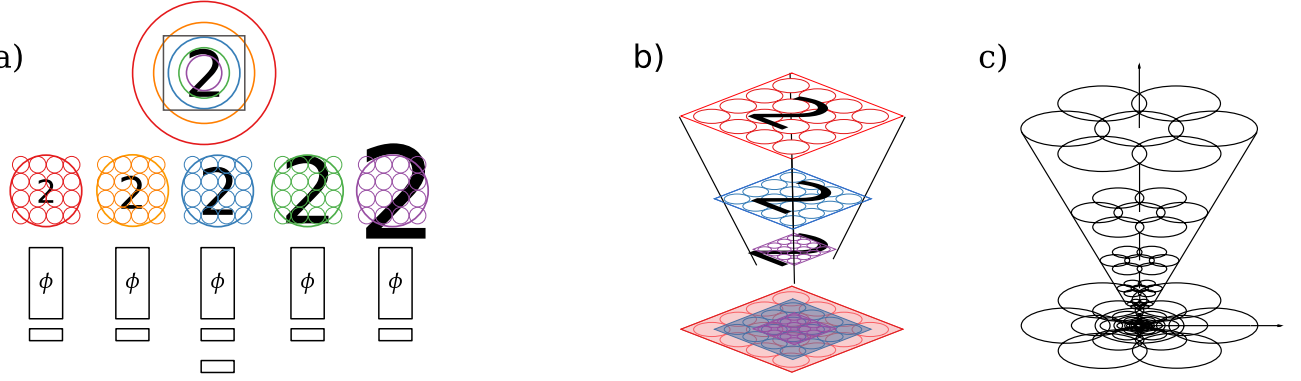


Fig. 2: *Foveated scale channel networks*. (a) Foveated scale channel network that process an image of the digit 2. Since each scale channel has a fixed size receptive field/support region in the scale channels, they will together process input regions corresponding to varying sizes in the original image (circles of corresponding colors). (b) This corresponds to a type of foveated processing, where the center of the image is processed with high resolution, which works well to detect small objects, while larger regions are processed using gradually reduced resolution, which enables detection of larger objects. (c) There is a close similarity between this model and the foveal scale space model [103], which was motivated by a combination of regular scale space axioms with a complementary assumption of a uniform limited processing capacity at all scales.

A scale channel network invariant to the continuous group of uniform scaling transformations $S = \{s \in \mathbb{R}_+\}$ can be constructed using an *infinite* set of scale channels $\{\phi_s\}_{s \in S}$. The following analysis also holds for a set of scale channels corresponding to a discrete subgroup of the group of uniform scaling transformations such that $S = \{\gamma^i | i \in \mathbb{Z}\}$, $\gamma > 1$.

The final output Λf from the scale channel network is an aggregation across the scale dimension of the last layer scale channel feature maps. In our theoretical treatment, we combine the output of the scale channels by the supremum

$$(\Lambda_{\sup} f)(x, c) = \sup_{s \in S} [(\phi_s f)(x, c, s)]. \quad (10)$$

Other permutation invariant operators such as averaging operations, could also be used. For this construction, the network output will be invariant to *rescalings around* $x_0 = 0$ for all x such that $(\Lambda_{\sup} f)(x, c) = (\Lambda_{\sup} S_s f)(x, c)$ (global scale invariance). This architecture is appropriate when characterising a single centered object that might vary in scale and it is the main architecture we explore in this paper. Alternatively, one may instead pool over *corresponding image points* in the original image by operations of the form

$$(\Lambda_{\sup}^{\text{local}} f)(x, c) = \sup_{s \in S} \{(\phi_s f)(S_s x, c)\} \quad (11)$$

This descriptor instead has the invariance property

$$(\Lambda_{\sup}^{\text{local}} f)(x_0, c) = (\Lambda_{\sup}^{\text{local}} S_{s, x_0} f)(x_0, c) \quad \text{for all } x_0, \quad (12)$$

i.e. when scaling around an arbitrary image point, the output *at that specific point* does not change (local scale invariance). This property makes it more suitable to describe scenes with multiple objects.

3.4.1 Scale covariance

Consider a scale channel network Λ (10) that expands the input over the group of uniform scaling transformations S . We can relate the feature map representation $\Gamma^{(i)}$ for a scaled image copy $\mathcal{S}_t f$ for $t \in S$ and its original f in terms of operator notation as

$$\begin{aligned} (\Gamma^{(i)} \mathcal{S}_t f)(x, c, s) &= (\phi_s^{(i)} \mathcal{S}_t f)(x, c) \\ &= (\phi^{(i)} \mathcal{S}_s \mathcal{S}_t f)(x, c) = (\phi^{(i)} \mathcal{S}_{st} f)(x, c) \\ &= (\phi_{st}^{(i)} f)(x, c) = (\Gamma^{(i)} f)(x, c, st), \end{aligned} \quad (13)$$

where we have used the definitions (8) and (9) together with the fact that S is a group. A scaling of an image thus only results in a multiplicative shift in the scale dimension of the feature maps. A more general and more rigorous proof using an integral representation of the scale channel network is given in Section 3.5.

3.4.2 Scale invariance

Consider the scale channel network Λ_{\sup} (10) that selects the supremum over scales. We will show that Λ_{\sup} is scale invariant, i.e., that

$$(\Lambda_{\sup} \mathcal{S}_t f)(x, c) = (\Lambda_{\sup} f)(x, c). \quad (14)$$

First, (13) gives $\{\phi_s^{(i)}(\mathcal{S}_t f)\}_{s \in S} = \{\phi_{st}^{(i)}(f)\}_{s \in S}$. Then, we note that $\{st\}_{s \in S} = St = S$. This holds both in the case when $S = \mathbb{R}_+$ and in the case when $S = \{\gamma^i | i \in \mathbb{Z}\}$. Thus,

we have

$$\begin{aligned} \{(\phi_s^{(i)} \mathcal{S}_t f)(x, c)\}_{s \in S} &= \{(\phi_{st}^{(i)} f)(x, c)\}_{s \in S} \\ &= \{(\phi_s^{(i)} f)(x, c)\}_{s \in S}, \end{aligned} \quad (15)$$

i.e. the set of outputs from the scale channels for a transformed image is equal to the set of outputs from the scale channels for its original image. For any permutation invariant aggregation operator, such as the supremum, we have that

$$\begin{aligned} (\Lambda_{\sup} \mathcal{S}_s f)(x, c) &= \sup_{s \in S} \{(\phi_{st}^{(k)} f)(x, c)\} \\ &= \sup_{s \in S} \{(\phi_s^{(k)} f)(x, c)\} = (\Lambda_{\sup} f)(x, c), \end{aligned} \quad (16)$$

and, thus, Λ is invariant to uniform rescalings.

3.5 Proof of scale and translation covariance using an integral representation of a scale channel network

We, here, prove the transformation property

$$(\Gamma^{(i)} h)(x, s, c) = (\Gamma^{(i)} f)(x + S_s S_t x_1 - S_t x_2, st, c) \quad (17)$$

of the scale channel feature maps under a more general combined scaling transformation and translation of the form

$$h(x') = f(x) \quad \text{for} \quad x' = S_t(x - x_1) + x_2 \quad (18)$$

corresponding to

$$h(x) = f(S_t^{-1}(x - x_2) + x_1) \quad (19)$$

using an integral representation of the deep network. In the special case when $x_1 = x_2 = x_0$, this corresponds to a uniform scaling transformation around x_0 (i.e. $S_{x_0, s}$). With $x_1 = x_0$ and $x_2 = x_0 + \delta$, this corresponds to a scaling transformation around x_0 followed by a translation \mathcal{D}_δ .

Consider a deep network $\phi^{(i)}$ (6) and assume the integral representation (7), where we for simplicity of notation incorporate the offsets $b_{i,c}$ into the non-linearities $\sigma_{i,c}$. By expanding the integral representation of the rescaled image h (19), we have that that the feature representation in the scale channel network is given by (with $M_0 = 1$ for a scalar input image):

$$\begin{aligned} (\Gamma^{(i)} h)(x, s, c) &= \{\text{definition (9)}\} = (\phi_s^{(i)} h)(x, c) \\ &= \{\text{definition (8)}\} = (\phi^{(i)} h_s)(x, c) = \{\text{equation (6)}\} \\ &= (\theta^{(i)} \theta^{(i-1)} \dots \theta^{(2)} \theta^{(1)} h_s)(x, c) = \{\text{equation (7)}\} \\ &= \sigma_{i,c} \left(\sum_{m_i=1}^{M_{i-1}} \int_{\xi_i \in \mathbb{R}^N} \sigma_{i-1, m_i} \left(\sum_{m_{i-1}=1}^{M_{i-2}} \int_{\xi_{i-1} \in \mathbb{R}^N} \dots \right. \right. \\ &\quad \left. \left. \sigma_{1, m_2} \left(\sum_{m_1=1}^{M_0} \int_{\xi_1 \in \mathbb{R}^N} h_s(x - \xi_i - \xi_{i-1} - \dots - \xi_1) \times \right. \right. \right. \\ &\quad \left. \left. \left. g_{m_1, m_2}^{(1)}(\xi_1) d\xi_1 \right) \dots g_{m_{i-1}, m_i}^{(i-1)}(\xi_{i-1}) d\xi_{i-1} \right) \\ &\quad \left. g_{m_i, c}^{(i)}(\xi_i) d\xi_i \right). \end{aligned} \quad (20)$$

Under the scaling transformation (18), the part of the integrand $h_s(x - \xi_i - \xi_{i-1} - \dots - \xi_1)$ transforms as follows:

$$\begin{aligned} h_s(x - \xi_i - \xi_{i-1} - \dots - \xi_1) &= \{h_s(x) = h(S_s^{-1}x) \text{ according to definition (2)}\} \\ &= h(S_s^{-1}(x - \xi_i - \xi_{i-1} - \dots - \xi_1)) \\ &= \{h(x) = f(S_t^{-1}(x - x_2) + x_1) \text{ according to (19)}\} \\ &= f(S_t^{-1} S_s^{-1}((x - \xi_i - \xi_{i-1} - \dots - \xi_1) - S_s x_2 + S_s S_t x_1)) \\ &= \{S_s S_t = S_{st} \text{ for scaling transformations}\} \\ &= f(S_{st}^{-1}((x + S_s S_t x_1 - S_s x_2 - \xi_i - \xi_{i-1} - \dots - \xi_1))) \\ &= \{f_{st}(x) = f(S_{st}^{-1}x) \text{ according to definition (2)}\} \\ &= f_{st}(x + S_s S_t x_1 - S_s x_2 - \xi_i - \xi_{i-1} - \dots - \xi_1). \end{aligned} \quad (21)$$

Inserting this transformed integrand into the integral representation (20) gives

$$\begin{aligned} (\Gamma^{(i)} h)(x, s, c) &= \\ &= \sigma_{i,c} \left(\sum_{m_i=1}^{M_{i-1}} \int_{\xi_i \in \mathbb{R}^N} \sigma_{i-1, m_i} \left(\sum_{m_{i-1}=1}^{M_{i-2}} \int_{\xi_{i-1} \in \mathbb{R}^N} \dots \right. \right. \\ &\quad \left. \left. \sigma_{1, m_2} \left(\sum_{m_1=1}^{M_0} \int_{\xi_1 \in \mathbb{R}^N} f_{st}(x + S_s S_t x_1 - S_s x_2 - \right. \right. \right. \\ &\quad \left. \left. \left. \xi_i - \xi_{i-1} - \dots - \xi_1) \times \right. \right. \right. \\ &\quad \left. \left. \left. g_{m_1, m_2}^{(1)}(\xi_1) d\xi_1 \right) \dots g_{m_{i-1}, m_i}^{(i-1)}(\xi_{i-1}) d\xi_{i-1} \right) \\ &\quad \left. g_{m_i, c}^{(i)}(\xi_i) d\xi_i \right), \end{aligned} \quad (22)$$

which we recognise as

$$\begin{aligned}
 & (\Gamma^{(i)} h)(x, s, c) \\
 &= (\theta^{(i)} \theta^{(i-1)} \dots \theta^{(2)} \theta^{(1)} f_{st})(x + S_s S_t x_1 - S_s x_2, c) \\
 &= (\phi^{(i)} f_{st})(x + S_s S_t x_1 - S_s x_2, c) \\
 &= (\phi_{st}^{(i)} f)(x + S_s S_t x_1 - S_s x_2, c) \\
 &= (\Gamma^{(i)} f)(x + S_s S_t x_1 - S_s x_2, st, c)
 \end{aligned} \tag{23}$$

and which proves the result. Note that for a pure translation ($S_t = I$, $x_1 = x_0$ and $x_2 = x_0 + \delta$) this gives

$$(\Gamma^{(i)} \mathcal{D}_\delta f)(x, c, s) = (\Gamma^{(i)} f)(x - S_s \delta, s, c). \tag{24}$$

Thus, translation covariance is preserved in the scale channel network but the magnitude of the spatial shift in the feature maps will depend on the scale channel.

3.6 Relations to scale-space theory

In classical scale-space theory [65, 66, 67, 68, 69, 70, 71, 72, 73, 74, 75], a multi-scale representation of an input image is created by convolving the image with a set of rescaled and normalised Gaussian kernels. The scale channel networks described in this paper are based on a similar philosophy of processing an image at *all scales simultaneously*, although the *input image*, as opposed to the filter, is expanded over scales.

For continuous image data, a representation computed by applying a fixed size filter to a set of rescaled input images is computationally equivalent to applying a set of rescaled and scale-normalised filters to a fixed size input (as done when computing a Gaussian scale-space representation). The two representations are related through a *spatial rescaling* and an *inverse mapping of the scale parameter* $s \mapsto s^{-1}$ (see Appendix A).

For discrete image data, a similar relation holds approximately, provided that the discrete rescaling operation is a sufficiently good approximation of the continuous rescaling operation.

A key difference compared to classical scale-space representations is that *non-linear* feature extractors *learned from data* are used as opposed to the mathematically derived Gaussian derivatives and differential invariants. The outputs from the scale channels do, however, still constitute a (*non-linear*) *scale-covariant multi-scale representation*, which implies that, *e.g.*, maxima over scale are preserved, although shifted to a different scale channel, when an input image is rescaled.

The use of *supremum*, or for a discrete set of scale channels, *max-pooling*, (see further Section 4) over the outputs of the scale channels is structurally similar to classical methods for *scale selection*, which detect maxima over scale of scale-normalised filter responses [7, 8, 104]. Here, max pooling

is, however, done over more complex feature responses, already adapted to detect specific objects, while classical scale selection is performed in a class-agnostic way based on low-level features. This makes max-pooling in the scale channel networks also closely related to more specialised classical methods that detect maxima from the scales at which a supervised classifier delivers class labels with the highest posterior [105, 106]. Average pooling over the outputs of a discrete set of scale channels (Section 4) is structurally similar to methods for scale selection that are based on *weighted averages* of filter responses at different scales [107, 18]. Although there is no guarantee that the learned non-linear features will, indeed, take maxima for relevant scales, one might expect training to promote this, since a failure to do so should be detrimental to the classification performance of these networks.

In case the learned features correspond to partial *Gaussian derivatives* of some orders, then the application of these filters to all the scale channels is, in fact, computationally equivalent to applying corresponding *scale-normalised Gaussian derivatives* to the original image (see Appendix B).

4 Discrete scale channel networks

Discrete scale channel networks are implemented by using a standard discrete CNN as the base network ϕ . For practical applications, it is also necessary to restrict the network to include a finite number of scale channels

$$\hat{S} = \{\gamma^i\}_{-K_{\min} \leq i \leq K_{\max}}. \tag{25}$$

The input image $f : \mathbb{Z}^2 \rightarrow \mathbb{R}$ is assumed to be of finite support. The outputs from the scale channels are, here, aggregated using, *e.g.*, max pooling

$$(\Lambda_{\max} f)(x, c) = \max_{s \in \hat{S}} \{(\phi_s f)(x, c, s)\} \tag{26}$$

or average pooling

$$(\Lambda_{\text{avg}} f)(x, c) = \text{avg}_{s \in \hat{S}} \{(\phi_s f)(x, c, s)\}. \tag{27}$$

We will also implement discrete scale channel networks that concatenate the outputs from the scale channels, followed by an additional transformation $\varphi : \mathbb{R}^{M_i |\hat{S}|} \rightarrow \mathbb{R}^{M_i}$ that mixes the information from the different channels

$$\begin{aligned}
 & (\Lambda_{\text{conc}} f)(x, c) \\
 &= \varphi \left([(\phi_{s_1} f)(x, c), (\phi_{s_2} f)(x, c) \dots (\phi_{s_{|\hat{S}|}} f)(x, c)] \right).
 \end{aligned} \tag{28}$$

Λ_{conc} does not have any theoretical guarantees of invariance, but since scale concatenation of outputs from the scale channels has been previously used with the explicit aim of scale invariant recognition [37], we will evaluate that approach also here.

4.1 Foveated processing

A standard convolutional neural network ϕ has a finite support region Ω in the input. When rescaling an input image of fixed size/finite support in the scale channels, it is necessary to decide how to process the resulting images of varying size using a feature extractor with fixed support. One option is to process regions of *constant size* in the scale channels corresponding to regions of *different sizes* in the input image. This results in *foveated image operations*, where a smaller region around the center of the input image is processed with high resolution, while gradually larger regions of the input image are processed with gradually reduced resolution (see Figure 2(b)-(c)). We will refer to the foveated network architectures Λ_{\max} , Λ_{avg} and Λ_{conc} as the FovMax network, the FovAvg network and the FovConc network, respectively.

4.2 Approximation of scale invariance

Foveated processing combined with max or average pooling will give an approximation of scale invariance in the continuous model (Section 3.4.2) over a *limited scale range*. The numerical scale warpings of the input images in the scale channels approximate continuous scaling transformations. A discrete set of scale channels will approximate the representation for a continuous scale parameter, where the approximation will be better with denser sampling of the scaling group.

A possible source to problems will, however, arise due to boundary effects caused by a finite scale interval. True scale invariance is only guaranteed for an infinite number of scale channels, since for a finite scale range there is a risk that the maximum value over the scale channels moves in or out of the finite scale interval because of scaling transformations, in the case of max pooling over the scale channels. Correspondingly, in the case of average pooling, there is a risk that a substantial part of mass of the feature responses from the different scale channels may move in or out of a finite scale interval, thus affecting the classification result from the scale channel network. The risk for such boundary effects can, however, be mitigated if the network would learn to suppress responses for both very zoomed in and very zoomed out objects, so that the contributions from such image structures are close to zero. As design criterion for scale channel networks, we therefore propose to include a sufficiently large number of scale channels both below and above the effective training scales of the relevant image structures and also training the network from scratch. Then, we propose that it should be likely that the network will learn to associate low values of the feature maps for such irrelevant image structures, that are off in scale, since the network would otherwise classify based on use of object views that will hardly provide any useful information.

4.3 Sliding window processing in the scale channels

An alternative option for dealing with varying image sizes is to, in each scale channel, process the entire rescaled image by applying the base network in a *sliding window manner*. The output from the scale channels can then be combined by max (or average) pooling over space followed by max (or average) pooling over scales

$$(\Lambda_{sw,\max} f)(c) = \max_{s \in S} \max_{x \in \Omega_s} \{(\phi_s f)(x, c, s)\}, \quad (29)$$

where $\Omega_s = \{sx | x \in \Omega\}$. We will here only evaluate the architecture using max pooling, which is structurally similar to the popular multi-scale OverFeat detector [48]. This network will be referred to as the SWMax network.

For this scale channel network to support invariance, it is not sufficient that boundary effects resulting from using a finite number of scale channels are mitigated. When processing regions in the scale channels corresponding to only a single region in the input image, new structures can appear (or disappear) in this region for a rescaled version of the original image. With a linear approach, this might be expected to not cause problems,³ since the best matching pattern will be the one corresponding to the template learned during training. For a deep neural network, however, there is no guarantee that there cannot be strong erroneous responses for, e.g., a partial view of a zoomed in object. We are, here, interested in studying the effects that this has on generalisation in the deep learning context.

5 Experiments on the MNIST Large Scale dataset

5.1 The MNIST Large Scale dataset

To evaluate the ability of standard CNNs and scale channel networks to generalise to unseen scales over a *wide scale range*, we have created a new version of the standard MNIST dataset [108]. This new dataset, *MNIST Large Scale*, which is available online [109], is composed of images of size 112×112 with scale variations of a factor 16 for scale factors $s \in [0.5, 8]$ relative to the original MNIST dataset (see Figure 3). The training and testing sets for the different scale factors are created by resampling the original MNIST training and testing sets using bicubic interpolation followed by smoothing and soft thresholding to reduce discretisation effects. Note that for scale factors > 4 , the full digit might not be visible in the image. These scale values are nonetheless

³ When using linear template matching, the best matching pattern for a template learned during training will be a very similar image patch. Thus, when sliding a template across a matching object it will take the maximum response when *centered* on the object. When using a non-linear method, however, there is no reason there could not be large responses for non centered views of familiar objects or completely novel patterns.

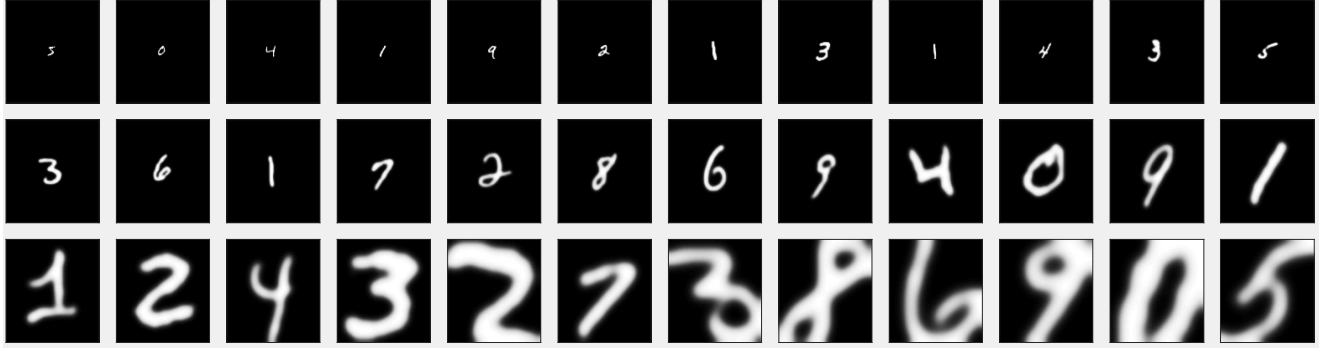


Fig. 3: *Samples from the MNIST Large Scale dataset*: The MNIST Large Scale dataset is derived from the original MNIST dataset [108] and contains 112×112 sized images of handwritten digits with scale variations of a factor of 16. The scale factors relative the original MNIST dataset are in the range $\frac{1}{2}$ (top left) to 8 (bottom right).

included to study the limits of generalisation. More details concerning this dataset are given in Appendix C.

5.2 Network and training details

In the experimental evaluation, we will compare five types of network designs: (i) a standard CNN, (ii) a FovMax scale channel network, (iii) a FovAvg scale channel network, (iv) a scale concatenation FovConc network and (v) a sliding window SWMax network:

The standard CNN is composed of 8 conv-batchnorm-ReLU blocks followed by a fully connected layer and a final softmax layer. The number of features/filters in each layer is 16-16-16-16-32-32-32-32-100-10. A stride of 2 is used in convolutional layers 2, 4, 6 and 8. The reason for using a quite deep network is to avoid a network structure that is heavily biased towards recognising either small or large digits.

The FovMax, FovAvg, FovConc and SWMax⁴ scale channel networks are constructed using scale channels with 4 conv-batchnorm-ReLU blocks followed by a fully connected layer and a final softmax layer. Rescaling within the scale channels is done with bilinear interpolation and applying border padding or cropping as needed. The batch normalisation layers are shared between the scale channels.

The number of features/filters in each layer is 16-16-32-32-100-10. A stride of 2 is used in convolutional layers 2 and 4. All the scale channel architectures have around 70 000 parameters, whereas the baseline CNN has around 90 000 parameters.

⁴ We noted that batch normalisation impairs the performance when training the SWMax network from scratch. We believe that this is because the sliding window approach implies a change in the feature distribution when processing data of different scales. For the batch normalisation to function optimally, the data/feature distribution should stay approximately the same. We, therefore, train the SWMax network without batch normalisation.

When computing the rescaled images used as input for the the scale channels, we used bilinear interpolation and border padding.

All the networks are trained with 50 000 training samples from the MNIST Large Scale dataset for 20 epochs using the Adam optimiser with default parameters in PyTorch: $\beta_1 = 0.9$ and $\beta_2 = 0.999$. During training, 15 % dropout is applied to the first fully connected layer. The learning rate starts at $3e^{-3}$ and decays with a factor $1/e$ every second epoch towards a minimum learning rate of $5e^{-5}$. Results are reported for the MNIST Large Scale testing set (10 000 samples) as the average of training each network using three different random seeds. The remaining 10 000 samples constitute a validation set. Numerical performance scores for the results in some of the figures to be reported are given in [110]

5.3 Generalisation to unseen scales

We, first, evaluate the ability of the standard CNN and the different scale channel networks to generalise to previously unseen scales. We train each network on either of the sizes 1, 2, and 4 from the MNIST Large Scale dataset and evaluate the performance on the testing set for scale factors between $1/2$ and 8. The FovMax, FovAvg and SWMax networks have 17 scale channels spanning the scale range $[\frac{1}{2}, 8]$. The FovConc network has 3 scale channels spanning the scale range $[1, 4]$.⁵ The results are presented in Figure 4. We, first, note that all the networks achieve similar top performance for the scales seen during training. There are, however, large

⁵ The FovConc network performs considerably worse when including too many scale channels or spanning a too wide scale range. Since we are more interested in the best case rather than the worst case scenario, we, here, picked the best network out of a large range of configurations.

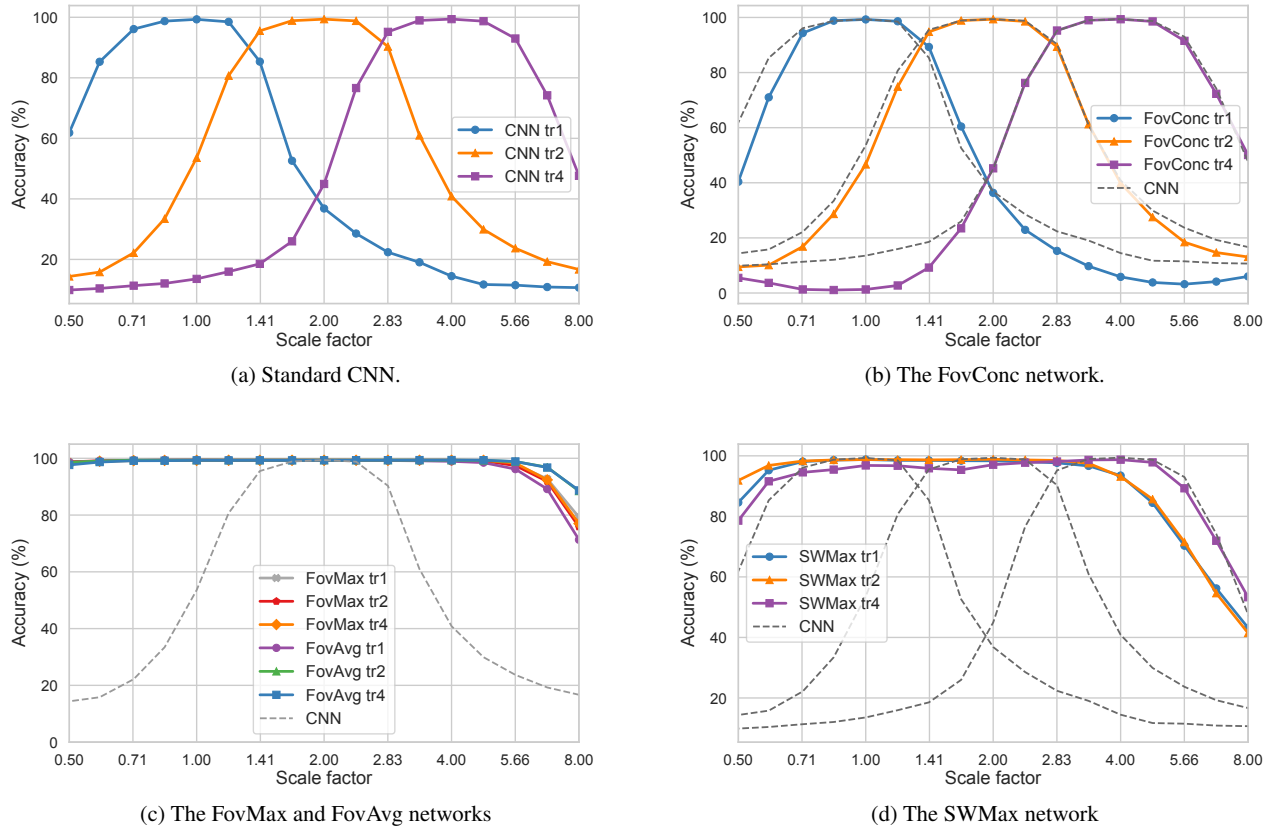


Fig. 4: *Generalisation ability to unseen scales for a standard CNN and the different scale channel network architectures for the MNIST Large Scale dataset.* The networks are trained on digits of size 1 (tr1), size 2 (tr2) or size 4 (tr4) and evaluated for varying rescalings of the testing set. We note that the CNN (a) and the FovConc network (b) have poor generalisation ability to unseen scales, while the FovMax and FovAvg networks (c) generalise extremely well. The SWMax network (d) generalises considerably better than a standard CNN, but there is some drop in performance for scales not seen during training.

differences in the abilities of the networks to generalise to unseen scales:

5.3.1 Standard CNN

The standard CNN shows limited generalisation ability to unseen scales with a large drop in accuracy for scale variations larger than a factor $\sqrt{2}$. This illustrates that, while the network can recognise digits of all sizes, a standard CNN includes no structural prior to promote scale invariance.

5.3.2 The FovConc network

The scale generalisation ability of the FovConc network is quite similar to that of the standard CNN, sometimes slightly worse. The reason why the scale generalisation is limited is that although the scale channels share their weights, when simply concatenating the outputs from the scale channels,

there is no structural constraint to support invariance. This is consistent with our observation that spanning a too wide scale range or using too many channels, the scale generalisation degrades for the FovConc network. For scales *not present during training*, there is, simply, no useful training signal to learn the correct weights in the fully connected layer that combines the outputs from the different scale channels. Note that our results are not contradictory to those previously reported for a similar network structure [37], since they train on data that contain natural scale variations and test over a quite narrow scale range. What we do show, however, is that this network structure is *not scale invariant*.

5.3.3 The FovAvg and FovMax networks

We note that the FovMax and FovAvg networks generalise very well, independently of what size the network is trained on. The maximum difference in performance in the size range

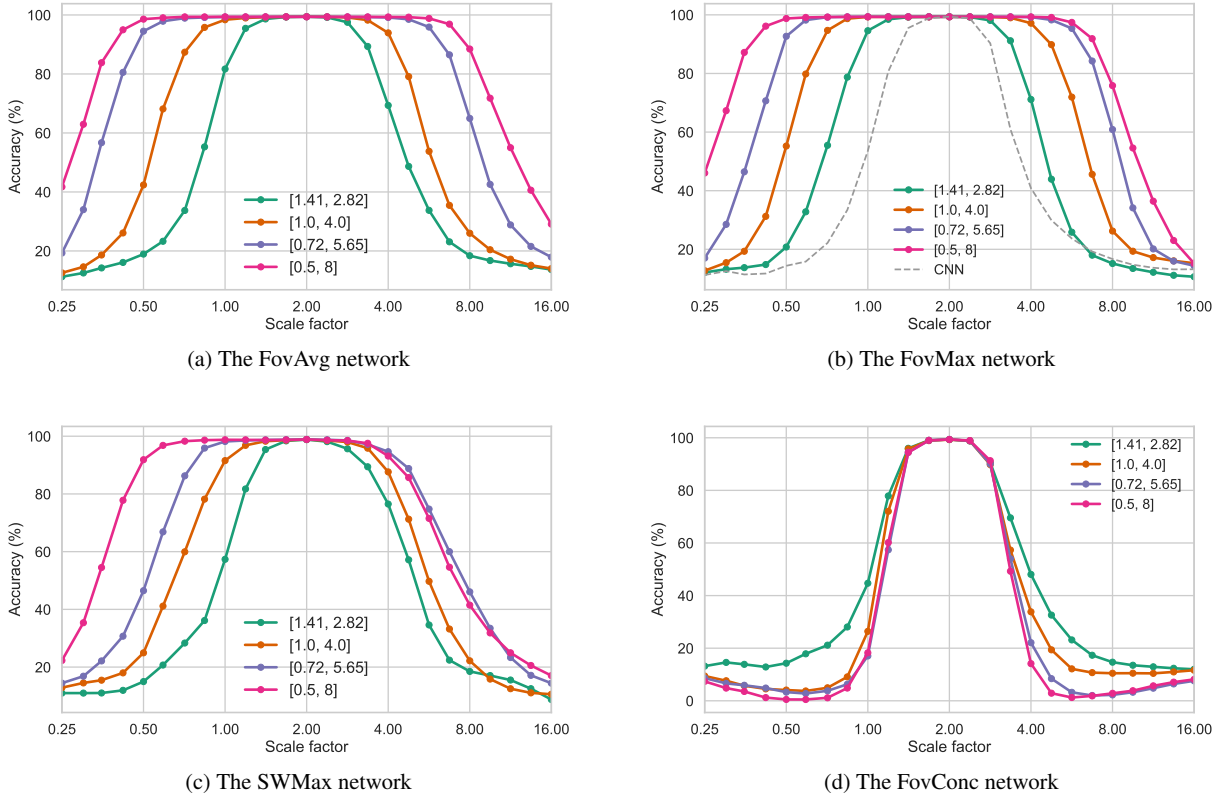


Fig. 5: Dependency of the scale generalisation property on the scale range spanned by the scale channels: (a)–(b) For the *FovAvg* and *FovMax* networks, the scale generalisation property is directly proportional to the scale range spanned by the scale channels, and there is no need to include training data for more than a single scale. (c) For the *SWMax* network, the scale generalisation is improved when including more scale channels, but the network does not generalise as well as the *FovAvg* and the *FovMax* networks. (d) For the *FovConc* network, the scale generalisation does actually become *worse* when including more scale channels (in the case of single-scale training), because there is no mechanism to support scale invariance when training the weights in the final fully connected layer that combines the different scale channels.

[1, 4] between training on size 1, size 2 or size 4 is less than 0.2 percentage points for these network architectures. Importantly, this shows that, if including a large enough number of scale channels and training the networks from scratch, boundary effects at the scale boundaries do not prohibit invariant recognition.

5.3.4 The *SWMax* network

We note that the *SWMax* network generalises considerably better than a standard CNN, but there is some drop in performance for sizes not seen during training. We believe that the main reason for this is, here, that since all scale channels are processing a fixed sized region in the input image (as opposed to for foveated processing), new structures might leave or enter this region when an image is rescaled. This might lead to erroneous high responses for unfamiliar views (see Section 4.3). We also noted that the *SWMax* networks

are harder to train (more sensitive to learning rate etc) compared to the foveated network architectures as well as more computationally expensive. Thus, while the *FovMax* and *FovAvg* networks still are easy to train and the performance is not degraded when spanning a wide scale range, the *SWMax* network seems to work best for spanning a more limited scale range, where fewer scale channels are needed (as was indeed the use case in [48]).

5.4 Dependency on the scale range spanned by the scale channels

Figure 5 shows the result of experiments to investigate the sensitivity of the scale generalisation properties to how wide range of scale values is spanned by the scale channels. For all the experiments, we have used a scale sampling ratio of $\sqrt{2}$ between adjacent scale channels. All the networks were

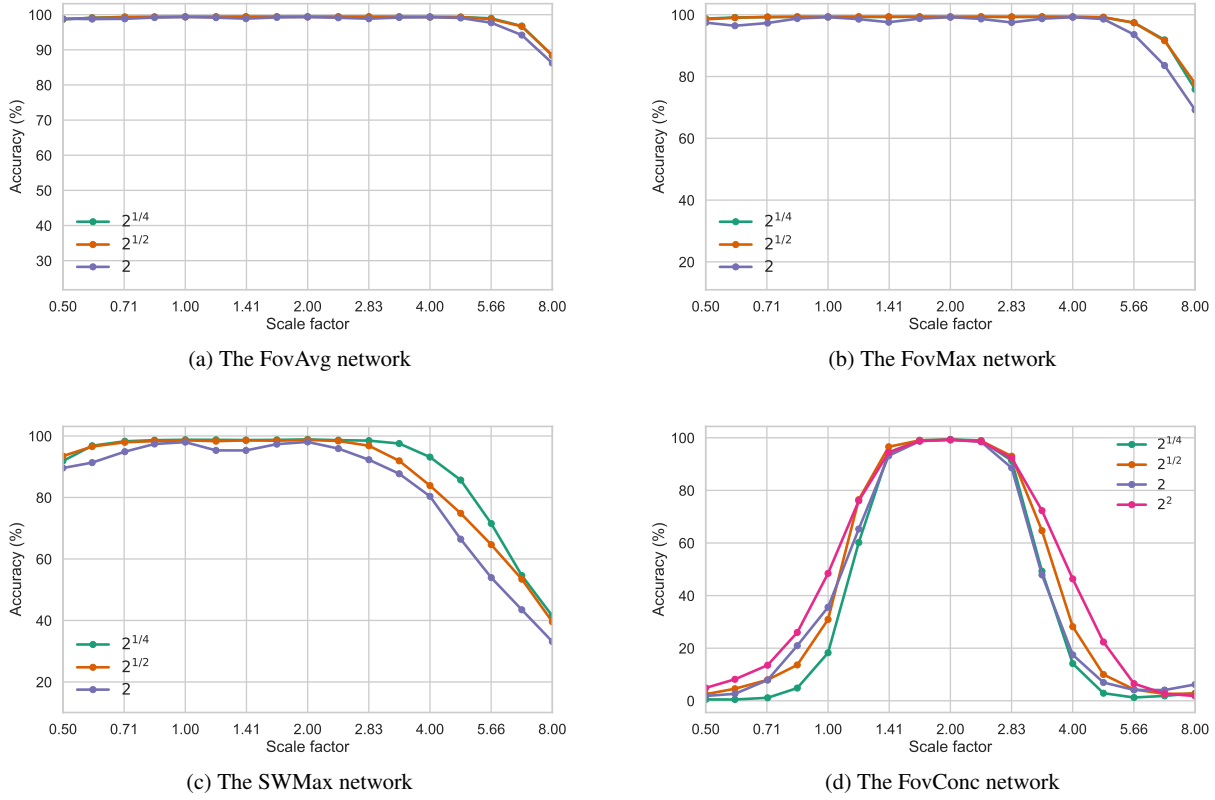


Fig. 6: *Dependency of the scale generalisation property on the scale sampling density*: (a)–(b) For the FovAvg and FovMax network, the overall scale generalisation is very good for all the the studied scale sampling rates, although it becomes noticeably better for $2^{1/2}$ compared to 2. For a more close up look regarding the *FovAvg* and *FovMax* networks, see Figure 7. (c) The SWMax network is more sensitive to how densely the scales are samples compared to the FovAvg and the FovMax networks, and the sensitivity to the scale sampling density is larger when observing objects that are *larger* than those seen during training, as compared to when observing objects that are *smaller* than those seen during training. (d) The FovConc network actually generalises worse with a denser sampling of scales. The reason for this is probably that for a dense sampling of scales, there is no need for the last fully connected layer (that processes the concatenated outputs from the scale channels) to include information from scales further away from the training scale. Thus, the weights corresponding to such scales may take arbitrary values without affecting the training accuracy, while implying very poor generalisation to unseen scales.

trained on the single size 2 and were tested for all sizes between $\frac{1}{2}$ and 8. The scale interval was varied between the four choices $[\sqrt{2}, 2\sqrt{2}]$, $[1, 4]$, $[1/\sqrt{2}, 4\sqrt{2}]$ and $[\frac{1}{2}, 8]$.

5.4.1 The FovAvg and FovMax networks

For the FovAvg and FovMax networks, the scale generalisation properties are directly connected to how wide scale range is spanned by the scale channels. By including more scale channels, these networks generalise over a wider scale range without any need to include training data for more than a single scale. The scale generalisation property will, however, be limited by the image resolution for small testing sizes and by the fact that the full object is not visible in the image for larger testing sizes.

5.4.2 The SWMax network

For the SWMax network, the scale generalisation property is improved when including more scale channels, but the network does not generalise as well as the FovAvg and the FovMax networks. It is also noticeable that scale generalisation is harder when for large testing sizes compared to small testing sizes. This is probably because of the problem with unfamiliar partial views present for sliding window processing becoming more pronounced for large testing sizes.

5.4.3 The FovConc network

For the FovConc network, the scale generalisation is actually *worse* when including more scale channels. This phe-

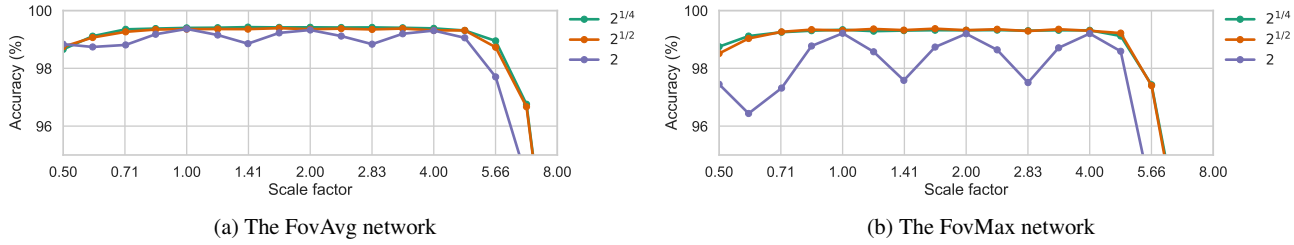


Fig. 7: *Dependency of the scale generalisation property on the scale sampling density for the FovAvg and FovMax networks:* FovMax and FovAvg networks spanning the scale range $[\frac{1}{4}, 8]$ were trained with varying spacing between the scale channels, either 2, $2^{1/2}$ or $2^{1/4}$. All the networks were trained on size 2. There is a significant increase in the performance when reducing the spacing between the scale channels from 2 to $2^{1/2}$, while the effect of a further reduction to $2^{1/4}$ is very small.

nomena can be understood by considering that the weights corresponding to the fully connected layer, that combines information from the concatenated scale channels output, are not controlled by any invariance mechanism. Indeed, the weights corresponding to scales not present during training may take arbitrary values without any significant impact on the training error. Incorrect weights for unseen scales will, however, imply very poor generalisation to unseen scales.

5.5 Dependency on the scale sampling density

Figure 6 and Figure 7 show the result of experiments to investigate the sensitivity of the scale generalisation property on the sampling density of the scale channels. All the networks were trained on size 2, with the scale channels spanning the scale range $[\frac{1}{2}, 8]$, and with a varying spacing between the scale channels: either 2, $2^{1/2}$ or $2^{1/4}$. For the FovConc network, we also included the spacing 2^2 .

The number of scale channels for the different sampling densities were for the 2^2 spacing: 3 channels, for the 2 spacing: 5 channels, for the $2^{1/2}$ spacing: 9 channels and for the $2^{1/4}$ spacing: 17 channels.

5.5.1 The FovAvg and FovMax networks

For both the FovAvg and FovMax networks, the accuracy is considerably improved when decreasing the ratio between adjacent scale levels from a factor 2 to a factor of $2^{1/2}$, while a further reduction to $2^{1/4}$ provides very low additional benefits.

5.5.2 The SWMax network

The SWMax network is more sensitive to how densely the scale levels are sampled compared to the FovAvg and FovMax networks. This sensitivity to the scale sampling density is larger, when observing objects of *larger size* than those

seen during training, as compared to when observing objects of *smaller size* than those seen during training.

This illustrates the problem due to partial views of objects, which will be present at some scales but not at others, are more severe when observing larger size objects than seen during training.

5.5.3 The FovConc network

The FovConc network does actually generalise worse with a denser sampling of scales. In fact, none of the network versions generalises better than a standard CNN. The reason for this is probably that for a dense sampling of scales, there is no need for the last fully connected layer, that processes the concatenated outputs from all the scale channels, to include information from scales further away from the training scale. Thus, the weights corresponding to such scales may take arbitrary values without affecting the accuracy during the training process, thereby implying very poor generalisation to previously unseen scales.

5.6 Multi-scale vs. single scale training

All the scale channel architectures support multi-scale processing although they might not support scale invariance. We, here, test the performance of the different scale channel networks when training on multi-scale training data. For comparison, we also investigate corresponding properties of the standard CNN.

5.6.1 Standard CNN

Figure 8 shows the result of training the standard CNN on training data with multiple sizes. Training is here performed for a uniform distribution of object sizes over the ranges $[1, 2]$ and $[2, 4]$, respectively, and testing on all sizes over the range $[\frac{1}{2}, 8]$. (The size distributions are uniform on a logarithmic scale.)

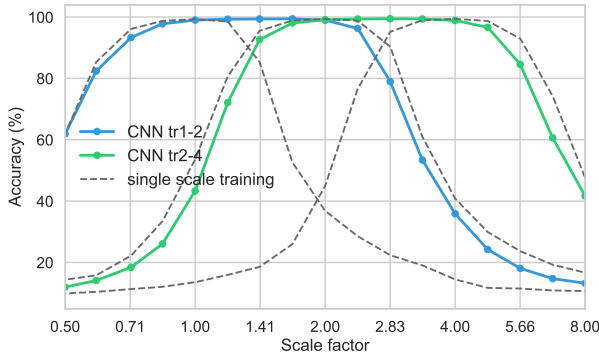


Fig. 8: *Comparing multi-scale vs. single-scale training for a vanilla CNN*. Training is here performed over the size ranges $[1, 2]$ and $[2, 4]$, respectively. The scale generalisation when trained on single size training data is presented as dashed grey lines for training sizes 1, 2 and 4, respectively. As can be seen from the results, training on multi-scale training data does not improve the scale generalisation ability of the CNN for sizes *outside the size range the network is trained on*.

As can be seen from the results, training on multi-scale training data does not improve the scale generalisation ability of the CNN for scales *outside the scale range the network is trained on*. The network can, indeed, learn to recognise digits of different sizes. But just because it might learn that an object of size 1 is the same as the same object of size 2, this does not at all imply that it will recognise the same object if it has size 4. In other words, the scale generalisation ability within a subrange does not transfer to outside that range.

5.6.2 The scale channel networks

Figure 9 shows the result of performing multi-scale training over the size range $[1, 4]$ for the scale channel networks FovMax, FovAvg, FovConc and SWMax.

For the FovMax, FovAvg and SWMax networks, we used the same scale channel setup (17 channels) as for single scale training. For the FovConc network, we used 5 scale channels spanning the scale range $[\frac{1}{2}, 8]$, since this setup gives better results compared to the previous setup with 3 channels.

As can be seen from the results, the difference between training on multi-scale and single scale data is striking for the FovConc network, as well as for the standard CNN shown for comparison. It can, however, be noted that the FovConc network generalises slightly better than a standard CNN outside the scale range it is trained on. When trained on multi-scale training data, the FovConc network works well, although with lower generalisation outside the scale range $[1, 4]$.

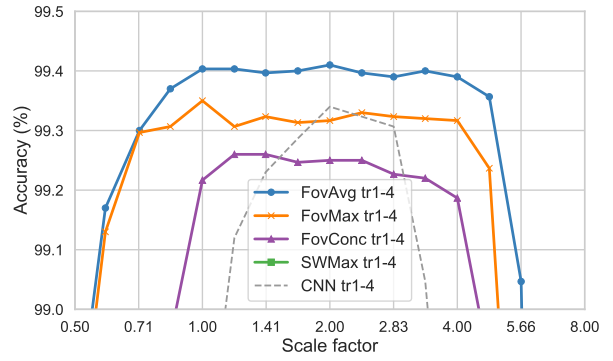
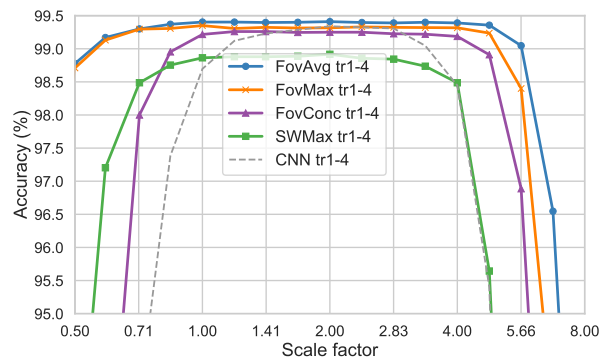
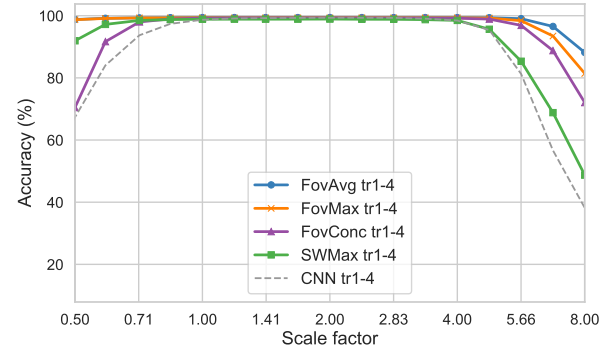


Fig. 9: *Results of multi-scale training for the scale channel networks with training sizes uniformly distributed on the size range $[1, 4]$ (with the uniform distribution on a logarithmic scale)*. These three figures show the same experimental results, although with a gradual zooming into more detailed properties of the graphs, to make comparisons between the networks more visible. The presence of multi-scale training data substantially improves the performance of the CNN, the FovConc network and the SWMax network, whereas the difference in performance between single-scale training and multi-scale training is almost indiscernable for the FovAvg and FovMax networks, illustrating the strong scale invariant properties of the FovAvg and FovMax networks. The overall best performance is also obtained for the FovAvg and FovMax networks.

Compact performance measures regarding scale generalisation on the MNIST Large Scale dataset

Scale range	[1/2, 1]	[1, 4]	[4, 8]	[1/2, 4]	[1/2, 8]
FovAvg 17ch tr1	99.15	99.27	90.82	99.22	96.76
FovAvg 17ch tr2	99.14	99.36	96.55	99.27	98.47
FovAvg 17ch tr4	98.78	99.31	96.61	99.11	98.36
FovAvg 17ch mean(tr1, tr2, tr4)	99.02	99.32	94.66	99.20	97.86
FovAvg 17ch tr14	99.20	99.40	96.50	99.32	98.49
FovMax 17ch tr1	99.15	99.35	93.70	99.27	97.63
FovMax 17ch tr2	99.15	99.31	92.72	99.25	97.32
FovMax 17ch tr4	99.03	99.30	93.26	99.20	97.45
FovMax 17ch mean(tr1, tr2, tr4)	99.11	99.32	93.23	99.24	97.47
FovMax 17ch tr14	99.16	99.32	94.37	99.26	97.82
FovConc 3ch tr1	80.76	48.64	4.61	57.10	44.68
FovConc 3ch tr2	22.35	78.17	22.71	59.12	49.55
FovConc 3ch tr4	2.57	50.20	82.36	35.64	45.63
FovConc 3ch mean(tr1, tr2, tr4)	35.23	59.00	36.56	50.62	46.62
FovConc 3ch tr14	91.66	99.24	91.16	96.32	94.64
SWMax 17ch tr1	95.06	97.60	69.52	96.53	88.77
SWMax 17ch tr2	96.87	97.96	69.28	97.48	89.44
SWMax 17ch tr4	91.40	97.23	82.21	95.02	91.04
SWMax 17ch mean(tr1, tr2, tr4)	94.44	97.60	73.67	96.34	89.75
SWMax 17ch tr14	97.05	98.82	79.40	98.13	92.60
CNN tr1	88.26	50.78	11.85	61.46	49.64
CNN tr2	27.87	79.88	26.08	61.90	52.60
CNN tr4	11.45	54.35	82.59	40.99	49.79
CNN mean(tr1, tr2, tr4)	42.53	61.67	40.17	54.78	50.68
CNN tr14	88.23	99.09	73.98	94.94	88.57

Table 1: Average classification accuracy (%) over different size ranges of the testing data. For each type of network (FovAvg, FovMax, FovConc, SW or CNN), this table shows the average classification accuracy over different ranges of the size of the testing data in the MNIST Large Scale datasets, for networks trained by single scale training for either of the training sizes 1, 2 or 4 (denoted tr1, tr2, tr4) or multi-scale training data spanning the scale range [1, 4] (denote tr14). The rows labelled “mean(tr1, tr2, tr4)” give the average value for the training sizes 1, 2 and 4. The reported accuracy is the average of the accuracy for multiple test sizes within the size ranges [1/2, 1], [1, 4], [4, 8], [1/2, 4] and [1/2, 8] with spacing $2^{1/4}$ between consecutive sizes.

Single-scale training evaluated over testing sizes in [1, 4]	
FovAvg mean(tr1, tr2, tr4)	99.32 %
FovMax mean(tr1, tr2, tr4)	99.32 %
SWMax mean(tr1, tr2, tr4)	97.60 %
CNN mean(tr1, tr2, tr4)	61.67 %
FovConc mean(tr1, tr2, tr4)	59.00 %

Table 2: Relative ranking of the different networks for single-scale training at either of the training sizes 1, 2 or 4 evaluated over the testing size interval [1, 4].

Multi-scale training evaluated over testing sizes in [1, 4]	
FovAvg tr14	99.40 %
FovMax tr14	99.32 %
FovConc tr14	99.24 %
CNN tr14	99.09 %
SWMax tr14	98.82 %

Table 3: Relative ranking of the different networks for multi-scale training over the training size interval [1, 4] evaluated over the testing size interval [1, 4].

Single-scale training evaluated over testing sizes in [1/2, 4]	
FovMax mean(tr1, tr2, tr4)	99.24 %
FovAvg mean(tr1, tr2, tr4)	99.20 %
SWMax mean(tr1, tr2, tr4)	96.34 %
CNN mean(tr1, tr2, tr4)	54.78 %
FovConc mean(tr1, tr2, tr4)	50.62 %

Table 4: Relative ranking of the different networks for single-scale training at either of the training sizes 1, 2 or 4 evaluated over the testing size interval [1/2, 4].

Multi-scale training evaluated over testing sizes in [1/2, 4]	
FovAvg tr14	99.32 %
FovMax tr14	99.26 %
SWMax tr14	98.13 %
FovConc tr14	96.32 %
CNN tr14	94.94 %

Table 5: Relative ranking of the different networks for multi-scale training over the training size interval [1, 4] evaluated over the testing size interval [1/2, 4].

and with slightly lower top performance compared to the FovAvg and FovMax networks. The FovConc network does, after all, include a mechanism for multi-scale processing and when trained on multi-scale training data, the lack of invariance mechanism in the fully connected layer is less of a problem for scales present during training.

For the SWMax network, including multi-scale data improves the scale generalisation somewhat for larger scales, but impairs the scale generalisation somewhat for smaller scales. The SWMax network does, however, have the worst performance for spanning larger scale ranges compared to the other networks. The reason behind this is probably that the multiple views produced in the different scale channels indeed makes the problem harder for this network compared to the foveated networks.

The difference in scale generalisation ability between training on a single scale or multi-scale image data is on the other hand almost indiscernible for the FovMax and FovAvg networks, although the FovAvg network is slightly improved by multi-scale training, illustrating the strong scale-invariant properties of the these networks.

5.7 Compact benchmarks regarding the scale generalisation performance

Table 6 gives compact performance measures of the generalisation performance of the different types of networks considered in the experiments on the MNIST Large Scale dataset. For each type of network (FovAvg, FovMax, FovConc, SW or CNN), the table gives the average classification accuracy over different ranges of the size of the testing data, for networks trained by single scale training, for either of the training sizes 1, 2 or 4 (denoted tr1, tr2, tr4), or multi-scale training data spanning the scale range [1, 4] (denoted tr14). The rows labelled “mean(tr1, tr2, tr4)” give the average value of performance values for the training sizes 1, 2 and 4.

Tables 2–5 gives relative ranking of the different networks on specific subsets of this data, which can be treated as benchmarks regarding scale generalisation for the MNIST Large Scale dataset. As can be seen from these tables, the FovAvg and FovMax networks have the overall best performance scores of these networks, both for the cases of single-scale training and multi-scale training.

The FovConc, CNN and SWMax networks are very much improved by multi-scale training, whereas the FovAvg and FovMax networks perform almost as well for single-scale training as for multi-scale training.

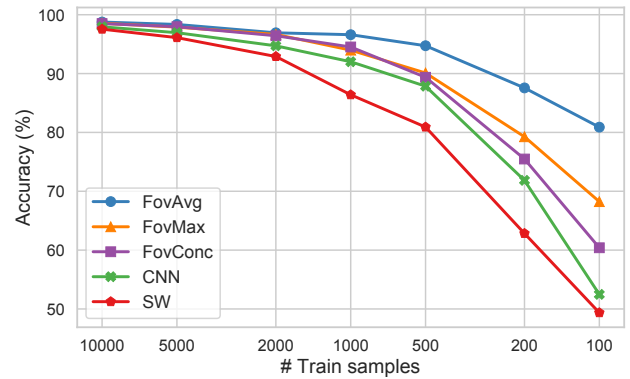


Fig. 10: *Training with smaller training sets with large scale variations.* All the network architectures are evaluated on their ability to classify data with large scale variations, while reducing the number of training samples. Both the training and the testing sets here span the size range [1, 4]. The FovAvg network shows the highest robustness when decreasing the number of training samples followed by the FovMax network. The FovConc network also shows a small improvement over the standard CNN.

5.8 Generalisation from fewer training samples

Another scenario of interest is when the training data does span a relevant range of scales, but there are few training samples. Theory would predict a correlation between the performance in this scenario and the ability to generalise to unseen scales.

To test this prediction, we trained the standard CNN and the different scale channel networks on multi scale training data spanning the size range [1, 4], while gradually reducing the number of samples in the training set. Here, the same scale channel setup with 17 channels spanning the scale range [$\frac{1}{2}$, 8] is used for all the architectures. The results are presented in Figure 10 and Table 6. We can note that the FovConc network shows some improvement over the standard CNN. The SWMax network, on the other hand, does not, and we hypothesise that when using fewer samples, the problem with partial views of objects (see Section 4.3) might be more severe. Note that the way the OverFeat detector is used in the original study [48] is more similar to our single scale training scenario, since they use base networks pre-trained on ImageNet. The FovAvg and FovMax networks show the highest robustness also in this scenario. This illustrates that these networks can give improvements when multi-scale training data is available but there are few training samples.

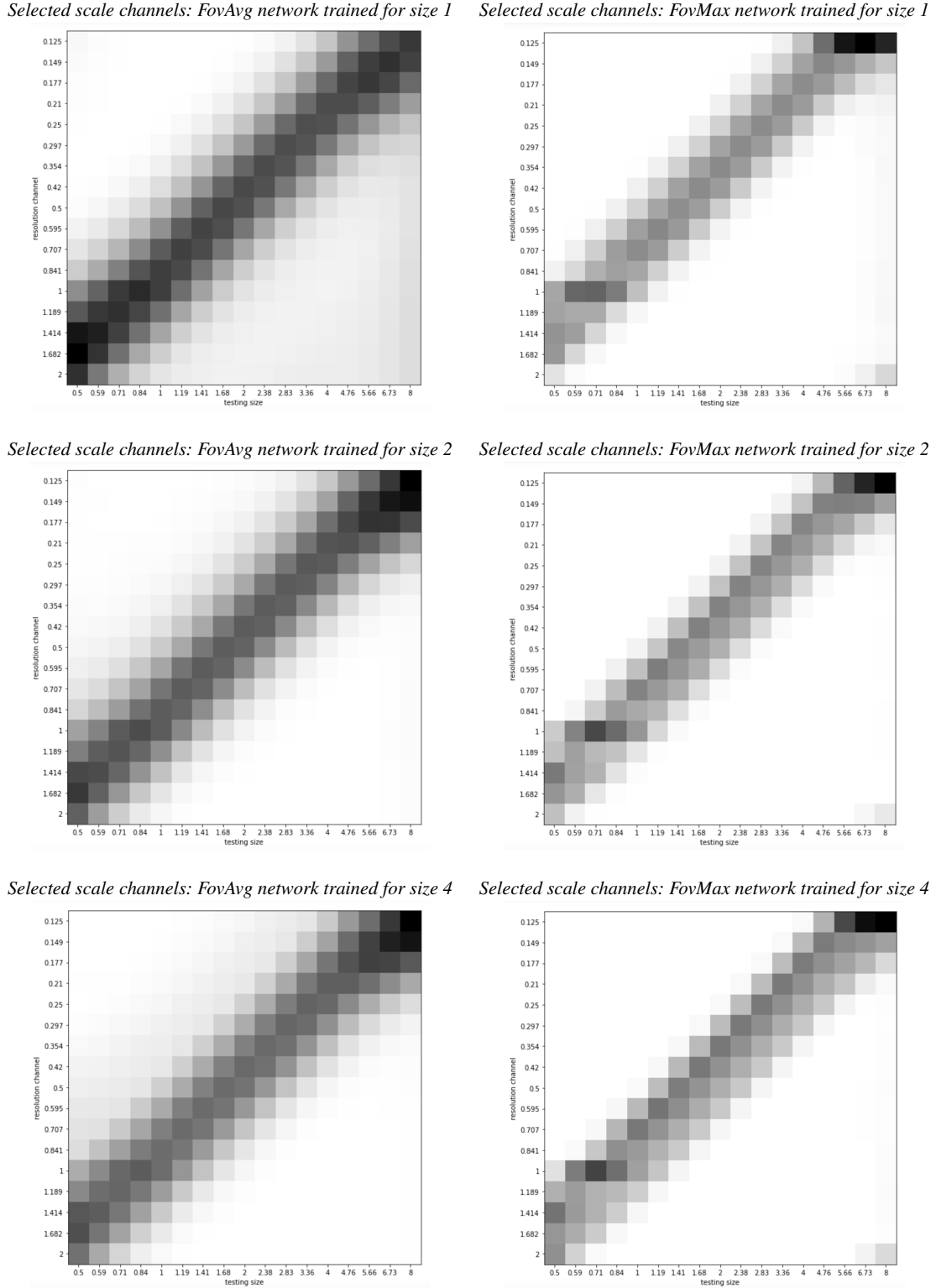


Fig. 11: Visualisation of the scale channels that contribute to each classification, when training the network for each one of the sizes 1, 2 and 4, for the scale-invariant FovAvg and FovMax networks. For each testing size, shown on the horizontal axis with increasing testing sizes towards the right, the vertical axis displays a histogram of the scale channels that contribute to the winning classification, with the lowest scale at the bottom and the highest scale at the top. As can be seen from the figures, there is a general tendency of the composed classification scheme to select coarser scale levels with increasing size of the image structures, in agreement with the conceptual similarity to classical methods for scale selection based on detecting local extrema over scale or performing weighted averaging over scale of scale-normalised derivative responses. (In these figures, the resolution parameter on the vertical axis represents the inverse of scale. Note that the grey-levels in the histograms are not directly comparable, since the grey-levels for each histogram are normalised with respect to the maximum and minimum values in that histogram.)

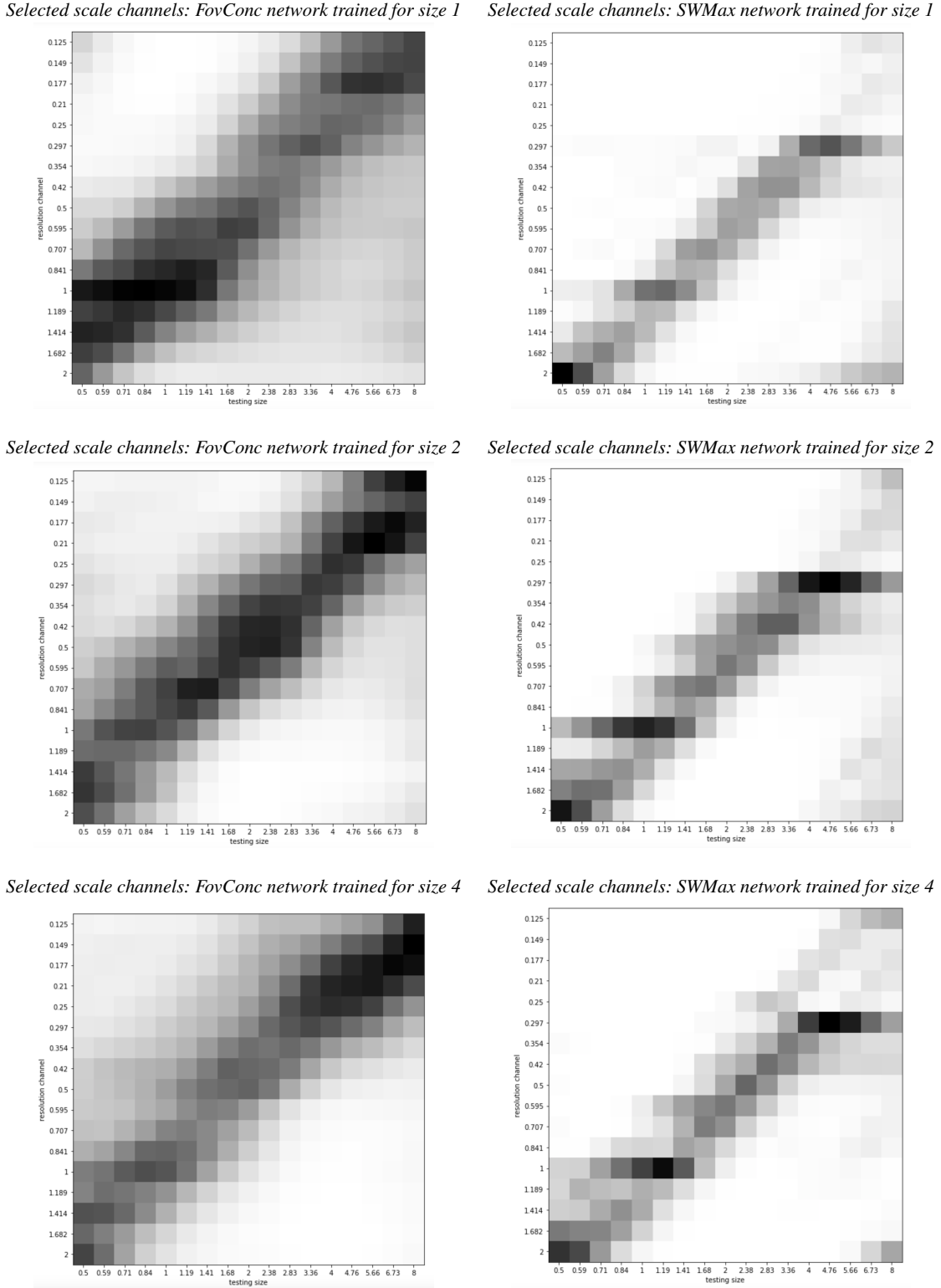


Fig. 12: Visualisation of the scale channels that contribute to each classification, when training the network for each one of the sizes 1, 2 and 4, for the not scale-invariant FovConc and SWMax networks. For each testing size, shown on the horizontal axis with increasing testing sizes towards the right, the vertical axis displays a histogram of the scale channels that contribute to the winning classification, with the lowest scale at the bottom and the highest scale at the top. As can be seen from the figures, the relative contributions from the different scale levels do not as well follow a linear dependency on the size of the input structures as for the scale-invariant FovAvg and FovConc networks. Instead, for the FovConc network, there is a bias towards the size of image structures used for training, whereas for the SWMax network some scale levels dominate for fine-scale or coarse-scale sizes in the testing data. (In these figures, the resolution parameter on the vertical axis represents the inverse of scale. Note that the grey-levels in the histograms are not directly comparable, since the grey-levels for each histogram are normalised with respect to the maximum and minimum values in that histogram.)

# samples	10 000	5 000	2 000	1 000	500	200	100
FovAvg 17ch	98.76	98.35	96.93	96.61	94.73	87.56	80.89
FovMax 17ch	98.56	97.89	96.66	93.98	90.10	79.26	68.24
FovConc 17ch	98.49	97.96	96.43	94.52	89.37	75.48	60.40
CNN	97.95	96.95	94.71	92.01	87.85	71.85	52.48
SWMax 17ch	97.55	96.11	92.90	86.40	80.91	62.83	49.36

Table 6: *Classification accuracy (%) as a function of the number of training samples when training on multi-scale training data.* The table shows the performance of the different network architectures when trained with a gradually reduced number of training samples from the MNIST Large Scale dataset (Figure 10). Both the training and the testing sets here span the size range [1, 4]. The FovAvg, FovMax, FovConc and SWMax networks all have 17 scale channels spanning the scale range $[\frac{1}{2}, 8]$. As can be seen, the FovAvg network shows the highest robustness when decreasing the number of training samples followed by the FovMax network.

5.9 Scale selection properties

To investigate which scale channels contribute most to the classification of digit in the MNIST Large Scale dataset as function of the size of the image structures in the input, we accumulated scale selection histograms for each one of the FovAvg, FovMax, FovConc and SWMax networks.

For the FovMax network, if the max pooling stage over the scale channels for the winning digit assumed its maximum over scale in a certain scale channel, we accumulated the bin in the histogram for that scale channel with a unit increment. Correspondingly for the FovAvg network, if the relative contribution from a scale channel for the winning digit was a fraction of unity for a scale channel, we incremented the histogram bin of that scale channel with the corresponding fraction of unity, in terms of absolute values of the relative contributions from the different scale channels.

For the FovConc network, we computed the relative contribution from each channel for the winning digit as the sum of the weights of fully connected layer multiplied by the contributions from each scale channel, and normalised the relative increment to a fraction of unity in terms of absolute values. For the SWMax network, if the max pooling stage over the scale channels for the winning digit was assumed in a certain scale channel, we accumulated the histogram bin for that scale channel with a unit increment.

This procedure was repeated for all the testing sizes in the MNIST Large Scale dataset, and in turn repeated for each one of the training sizes 1, 2 and 4, resulting in the two-dimensional scale selection histograms in Figures 11–12, which show what scale channels contribute to the classification output as function of the size of the image structures in the testing data.

As can be seen in Figure 11, the selected scale levels in these scale selection histograms do very well follow a linear trend for the FovAvg and FovMax networks, in the sense that the selected scale levels are proportional to the size of

the image structures in the testing data.⁶ The scale selection histograms are also largely similar, irrespective of whether the training is performed for size 1, 2 or 4, illustrating that the scale invariant properties of the FovAvg and FovMax networks in the continuous case transfer very well to the discrete implementation.

In this respect, the resulting scale selection properties of the FovAvg and FovMax networks share similarities to classical methods for scale selection based on local extrema over scale or weighted averaging over scale of scale-normalised derivative responses [7, 8, 107, 18, 104]. (As previously mentioned, and as shown in Appendix B, the scaling properties of the filters applied to the scale channels are similar to the scaling properties of scale-normalised Gaussian derivatives, that classical basic scale selection methods are based on.) The approach for the FovMax network is also closely related to the scale selection approach in [106, 111] based on choosing the scales at which a supervised classifier delivers class labels with the highest posterior.

As can be seen in Figure 12, the behaviour is different for the not scale-invariant FovConc and SWMax networks. For the FovConc network, there is a bias in that the selected scales are more concentrated towards the size of the training data. The contributions from the different scale chan-

⁶ A certain bias that can be observed for the FovMax and SWMax networks, is that there is a stronger peak in the histogram scale channels for scale channel 1 for small testing sizes, than for the neighbouring scale channels. A possible explanation for this effect is that for scale channel 1 there will not be any effective initial interpolation stage as for the other scale channels, which implies that there is no additional interpolation blur for this scale channel as for the other scale channels, in turn implying a stronger response for this scale channel compared to the neighbouring scale channels. A certain bias towards scale channel 1 can also be observed for the FovConc network. For the FovAvg network, which is also the network that performs clearly best out of these four networks, the bias towards scale channel 1 is, however, very minor. In retrospect, the bias towards scale channel 1 for the other networks could point to replacing the initial bilinear interpolation stage by some other interpolation method, and/or to add a small complementary smoothing stage after the interpolation stage, to ensure that the sum of the effective interpolation blur and the added complementary blur remains approximately the same for neighbouring scale channels.

nels are also much less concentrated around the linear trend compared to the FovAvg and FovMax networks. Without access to multi-scale training, the FovConc network is not able to learn scale invariance, as would have been the result if the network could learn to use equal weights for all the scales, and in that way implement average pooling over scale, which in principle would be possible, given the degrees of freedom in the final fully connected layer. For the SWMax network, although the resulting scale selection histogram is largely centered around a linear trend, the linear trend is not as clean as for the FovMax network. For the coarsest scale testing structures, the SWMax network largely fails to activate corresponding scale channels beyond a certain value. This could be related to our previously noted problem for the SWMax network of choosing to classify based on zoomed-in previously unseen partial views instead of classifying based on the zoomed-out overall shape. Furthermore, for finer or coarser scale testing structures, there are some scale channels for the SWMax network that contribute more to the output than others, and thus demonstrate a lack of true scale invariance.

In the quantitative scale generalisation experiments presented earlier, we showed that this lack of scale invariance leads to lower accuracy when the FovConc and SWMax networks attempt to perform scale generalisation, whereas the truly scale-invariant FovAvg and FovMax networks have excellent scale generalisation properties.

6 Experiments on the CIFAR-10 Scale dataset

6.1 The CIFAR-10 Scale dataset

From the CIFAR-10 dataset [112], we created a scaled dataset, referred to as the CIFAR-10 Scale dataset, where the test images in the original CIFAR-10 dataset are rescaled with relative scale factors in the range $s \in [0.5, 2.0]$. This dataset represents a dataset where the conditions for invariance using scale channel network are not fulfilled, because the transformations between different training and testing sizes may not be well modelled by continuous scaling transformations, as underlie the presented theory for scale invariant scale channel networks, based on continuous models of both the image data and the image filtering operations.

Already the original CIFAR-10 dataset is at the limit of being undersampled. Thus, reducing the image size further for scale factors $s < 1$ results in additional loss of object details. The images are also tightly cropped, which implies that when increasing the image size for scale factors $s > 1$ implies a loss of information towards the image boundaries, and that sampling artefacts in the original image data will be further amplified. When reducing the image size, we extend the image by mirroring at the image boundaries, implying artefacts in the image structures, caused by the im-

age padding operations. The reason why we nevertheless include an experimental evaluation on this dataset, is to test the limits of the evaluated scale channel approach in a more challenging scenario, near or beyond the limits of image resolution, to see if a scale channel network can still provide a clear advantage over a standard CNN.

Figure 13 shows a few images from this dataset, with examples of two out of the 10 object classes in the dataset: “airplanes”, “cars”, “birds”, “cats”, “deer”, “dogs”, “frogs”, “horses”, “ships”, and “trucks”.

6.2 Network and training details

For the CIFAR-10 Scale dataset, we will compare the FovMax, FovAvg and FovConc networks to a standard CNN.⁷

For all the networks, the base network is a 7-layer network with conv+batchnorm+ReLU layers with zero padding with width 1. We do not use any spatial max pooling, but a stride of 2 for convolutional layers 3, 5 and 7. Then, spatial average pooling is performed down to 1×1 resolution, followed by a final fully connected softmax layer. We do not use dropout, since it did not improve the results. All the convolutional layers consist of 3×3 filters.

For the FovAvg and FovMax networks, also max-pooling and average pooling, respectively, is performed across the scale channels, *i.e.*, after the softmax layer. For the FovConc network, we have a fully connected layer that combines the information from the multiple scale channels after the softmax layer.

The number of feature channels is 32-32-32-64-64-128-128 for the 7 convolutional layers.

When computing the rescaled images used as input for the scale channels, bilinear interpolation is performed relative to the original image and with reflection padding at the image boundaries.

All the CIFAR-10 networks are trained for 20 000 time steps using 50 000 training samples over 103 epochs, using a batch size of 256 and the Adam optimiser with default parameters in PyTorch: $\beta_1 = 0.9$ and $\beta_2 = 0.999$. A cosine learning rate decay is used with starting learning rate 0.001 and floor learning rate 0.00005, where the learning rate decreases to the floor learning rate after 75 epochs. The network is tested on the 10 000 images in the testing set, for relative scaling factors in the interval $[\frac{1}{2}, 2]$.

We chose the learning rate based on the CNN performance using the last 10 000 samples of the training set as a validation set.

⁷ We do not evaluate the SWMax network on the CIFAR-10 Scale dataset, since it is not meaningful to perform a spatial search for objects in this dataset.



Fig. 13: Sample images from the CIFAR-10 Scale dataset (of size 32×32 pixels). The test images from the original CIFAR-10 testing set are rescaled for scaling factors between $\frac{1}{2}$ and 2, with mirror extension at the image boundaries for scaling factors $s < 1$. Top row: “frog”. Bottom row: “truck”.

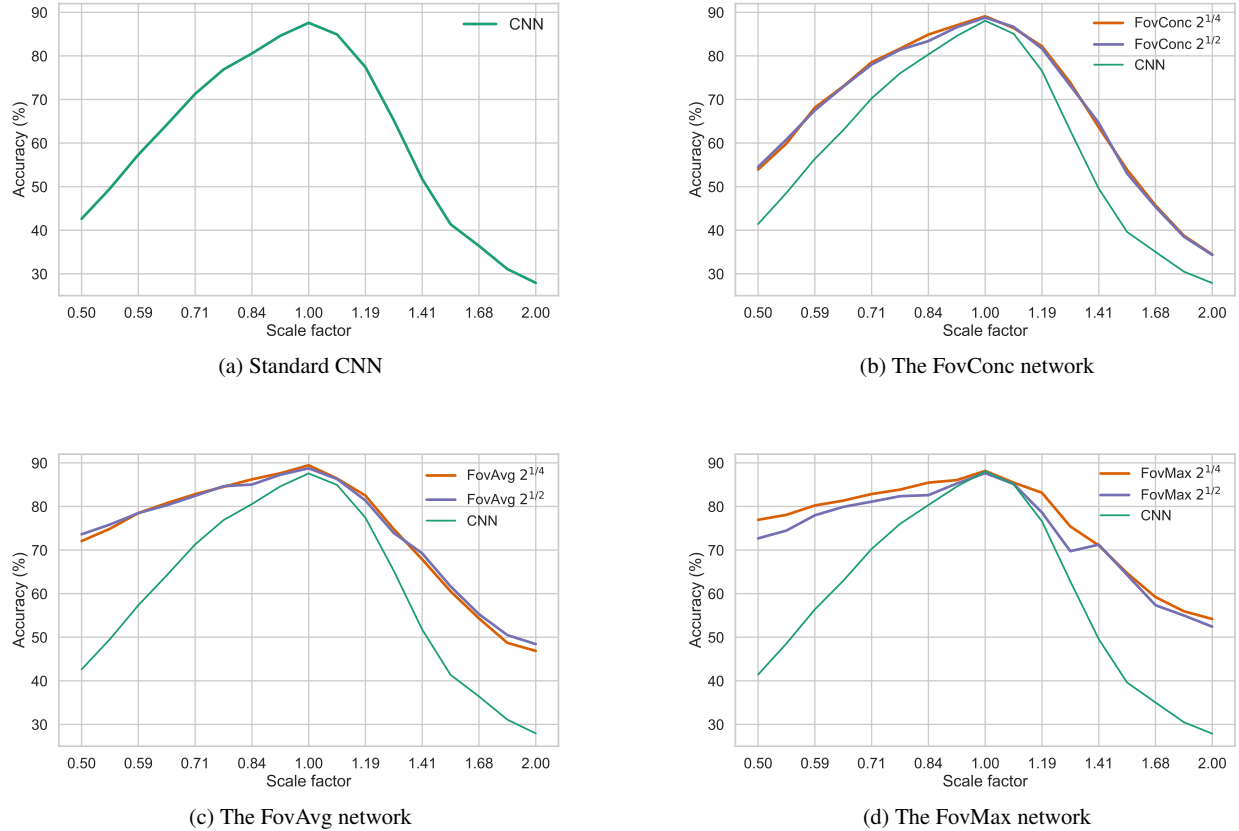


Fig. 14: Generalisation ability to unseen scales for a standard CNN and different scale channel network architectures for the CIFAR-10 Scale dataset. The network is trained on the standard CIFAR-10 training set (corresponding to scale factor 1.0) and tested on rescaled images from the testing set for relative scale factors between $\frac{1}{2}$ and 2. The FovConc network has better scale generalisation compared to the standard CNN, but for larger deviations from the scale that the network is trained on, there is a clear advantage for the FovAvg and the FovMax networks.

6.3 Experimental results

The results for the *standard CNN* are shown in Figure 14(a). It can be seen that, already for a scale factors slightly off from 1, there is a noticeable drop in generalisation performance.

The results for the *FovConc network*, for different number of scale channels are presented in Figure 14(b). The generalisation ability to new scales is markedly better than for the standard CNN, but the scale generalisation is not improved by adding more scale channels.

The results for the *FovMax and FovAvg networks*, for different numbers of scale channels, are presented in Figure 14(c-d), and are significantly better than for the standard CNN and the FovConc network. For the FovAvg network, the peak performance is slightly better than for the FovMax network. For the FovMax network, there is a noticeable improvement by going to a finer scale sampling ratio of $2^{1/4}$ compared to $2^{1/2}$. Then, the generalisation ability for the FovMax network is also better than for the FovAvg network.

A possible reason why the scale generalisation ability of the scale concatenation network outside the training set has a larger difference relative to a standard CNN for the CIFAR-10 dataset, compared to the previous MNIST data, is that for the CIFAR-10 dataset there are indeed some scale variations present in the training set, and as discussed earlier, it is possible for this network to learn to generalise by having assigning appropriate weights to the layer that combines information from the different scale channels. Limited scale generalisation ability might thus be learned from the dataset, where the scale channel structure implies the advantage of sharing parameters across scales and multi-scale processing of the image.

To summarise, the FovMax and FovAvg networks provide the best generalisation ability to new scales, which is in line with theory. Thus, also for datasets where the conditions regarding image size and resolution are not such that the scale channel approach can provide full invariance, the scale channel architecture can nevertheless provide benefits.

7 Summary and conclusions

We have presented a methodology to handle scaling transformations in deep networks by scale channel networks. Specifically, we have presented a theoretical formalism for modelling scale channel networks based on continuous models of the both the filters and the image data, and shown that the continuous scale channel networks are provably scale covariant and translationally covariant. Combined with max pooling or average pooling over the scale channels, our foveated scale channel networks are additionally provably scale invariant.

Experimentally, we have demonstrated that discrete approximations to the continuous foveated scale channel networks FovMax and FovAvg are robust to scaling transformations, and allow for scale generalisation, with very good performance for classifying image patterns at new scales not spanned by the training data, because of the continuous invariance properties that they approximate. Experimentally, we have also demonstrated limited scale generalisation performance of vanilla CNNs, scale concatenation networks and sliding window networks, when exposed to testing at scales not spanned by the training data, although those approaches may work rather well when training on multi-scale training data. The reason whey those approaches fail regarding scale generalisation, when trained at a single scale or a over a narrow scale interval only, is because of the lack of an explicit mechanism to enforce scale invariance.

We have also demonstrated that our FovMax and FovAvg scale channel networks lead to improvements when training on data with significant scale variations in the small sample regime. We have also shown that the selected scale levels for these scale invariant networks increase linearly with the size of the image structures in the testing data, in a similar way as for classical methods for scale selection.

From the presented experimental results, it is clear that our FovMax and FovAvg scale channel networks do provide a considerable improvement in scale generalisation ability compared to a standard CNN as well as in relation to previous scale channel approaches. Even in the presence of undersampling and serious boundary effects, our FovMax and FovAvg scale channel networks give considerably better generalisation ability compared to a standard CNN or alternative scale channel networks. We therefore believe that our proposed foveated scale channel networks could prove useful in situations where a simple approach that can generalise to unseen scales or learn from small datasets with large scale variations is needed. Strong reasons for using such scale-invariant scale channel networks could either be because there is a limited amount of multi-scale training data, where sharing statistical strength between scales is valuable, or because only a single scale or a limited range of scales is present in the training set, which implies that generalisation outside the scales seen during training is crucial for the performance. Thus, we propose that this type of foveated scale invariant processing could be included as subparts in more complex frameworks dealing with large scale variations.

A more overarching aim of this study have been to test the limits of CNNs to generalise to unseen scales over wide scale ranges. The key take home message is a proof of concept that such scale generalisation is possible, if including structural assumptions about scale in the network design.

Appendix

A Relations between scale channel networks and scale-space theory

We, here, discuss in more detail the relationship between the representations computed in a (continuous) scale channel network and the representations computed within classical scale-space theory. Although a multi-layer scale channel network will compute more complex non-linear features, it is enlightening to investigate whether the network could learn to express operations similar to those used within the classical scale-space paradigm. This will increase our confidence that scale channel networks could be expected to work well together with, *e.g.*, max-pooling over scales.

A.1 Preliminaries

In classical scale-space theory, a *scale-space representation* of an input image $f : \mathbb{R}^N \rightarrow \mathbb{R}$ is defined as [69]:

$$L(x; \sigma) = \int_{u \in \mathbb{R}^N} f(x - u) g(u; \sigma) du, \quad (30)$$

where $g : \mathbb{R}^N \times \mathbb{R}^+ \rightarrow \mathbb{R}$ denotes the (rotationally symmetric) Gaussian kernel

$$g(x; \sigma) = \frac{1}{(\sqrt{2\pi}\sigma)^N} e^{-\frac{x^2}{2\sigma^2}}, \quad (31)$$

and we use σ as the the *scale parameter* compared to the more commonly used $t = \sigma^2$. From this representation, a family of *Gaussian derivatives* can be computed as

$$L_{x^\alpha}(x; \sigma) = \partial_{x^\alpha} L(x; \sigma) = ((\partial_{x^\alpha} g(\cdot; \sigma)) * f(\cdot))(x), \quad (32)$$

where $n \in \mathbb{Z}$ and we use multi index notation $\alpha = (\alpha_1, \dots, \alpha_N)$ such that $\partial_{x^\alpha} = \partial_{x^{\alpha_1}} \dots \partial_{x^{\alpha_N}}$. The scale covariance property of the scale-space representation also transfers to such Gaussian derivatives, and these visual primitives have been widely used within the classical computer vision paradigm to construct scale-covariant and scale-invariant feature detectors and image descriptors [7, 8, 10, 11, 13, 14, 15, 16, 113, 18]. One way to achieve scale invariance is to first perform *scale selection* and then, *e.g.*, extract features at the identified scale. Scale selection can be done by comparing the magnitudes of γ -normalised derivatives [7, 8]:

$$\partial_{\xi^\alpha} = \partial_{x^\alpha, \gamma-norm} = t^{|\alpha|\gamma/2} \partial_{x^\alpha} = \sigma^{|\alpha|\gamma} \partial_{x^\alpha} \quad (33)$$

with $\gamma \in [0, 1]$ as a free parameter and $|\alpha| = \alpha_1 + \dots + \alpha_N$. Such derivatives are likely to take maxima at scales corresponding to the relevant physical scales of objects in the image. We will here consider the maximally scale-invariant case with $\gamma = 1$

$$\partial_{\xi^\alpha} = \sigma^{|\alpha|} \partial_{x^\alpha} \quad (34)$$

and show that scale channel networks will compute something similar to such scale-normalised derivatives. First, we will, however, consider the relationship between multi-scale representations computed by applying a set of *rescaled kernels* to a single scale image and representations computed by applying the same kernel to a set of *rescaled images*.

A.2 Scaling the image *vs.* scaling the filter

Since the scale-space representation can be computed using a single convolutional layer we, here, compare with a single layer scale-channel network. We consider the relationship between representations computed by:

- (i) Applying a set of rescaled and scale-normalised filters (this corresponds to normalising filters to constant L_1 -norm over scales) $h : \mathbb{R}^N \rightarrow \mathbb{R}$

$$h_s(x) = \frac{1}{s^N} h\left(\frac{x}{s}\right) \quad (35)$$

to a fixed size input image $f(x)$:

$$L_h(x; s) = (f * h_s)(x) = \int_{u \in \mathbb{R}^N} f(u) h_s(x - u) du, \quad (36)$$

where the subscript indicates that h might not necessarily be a Gaussian kernel. If h is a Gaussian then $L_h = L$.

- (ii) Applying a fixed size filter h to a set of rescaled input images

$$M_h(x; s) = (f_s * h)(x) = \int_{u \in \mathbb{R}^N} f_s(u) h(x - u) du, \quad (37)$$

with

$$f_s(x) = f\left(\frac{x}{s}\right). \quad (38)$$

This is the representation computed by a single layer in a (continuous) scale channel network.

It is straightforward to show that these representations are computationally equivalent and related by a family of scale dependent scaling transformations. We compute using the

change of variables $u = s v$, $du = s^N dv$:

$$\begin{aligned}
L_h(x; s) &= (f * h_s)(x) \\
&= \int_{u \in \mathbb{R}^N} f(x - u) \frac{1}{s^N} h\left(\frac{u}{s}\right) du \\
&= \int_{u \in \mathbb{R}^N} f(x - sv) \frac{1}{s^N} h(v) s^N dv \\
&= \int_{u \in \mathbb{R}^N} f\left(s\left(\frac{x}{s} - v\right)\right) h(v) dv \\
&= \int_{u \in \mathbb{R}^N} f_{s^{-1}}\left(\frac{x}{s} - v\right) h(v) dv \\
&= (f_{s^{-1}} * h)\left(\frac{x}{s}, s^{-1}\right).
\end{aligned} \tag{39}$$

Comparing this with (37) we see that the two representations are related according to

$$L_h(x; s) = M_h\left(\frac{x}{s}; s^{-1}\right). \tag{40}$$

We note that the relation (40) preserves *the relative scale* between the filter and the image for each scale and that both representations are scale covariant. Thus, to convolve a set of rescaled images with a single scale filter, as done in the scale channel networks, is computationally equivalent to convolving an image with a set of rescaled filters that are L_1 -normalised over scale. The two representations are related through a *spatial rescaling* and an *inverse mapping of the scale parameter* $s \mapsto s^{-1}$. Note that it is straightforward to show, using the integral representation of a scale channel network (7), that a corresponding relation between scaling the image and scaling the filters holds for a multi-layer scale channel network as well.

The result (40) implies that if a scale channel network learns a feature corresponding to a Gaussian with the standard deviation σ , then the representation computed by the scale channel network is computationally equivalent to applying the family of kernels

$$h_s(x) = \frac{1}{s^N} h\left(\frac{x}{s}\right) = \frac{1}{(\sqrt{2\pi}s\sigma)^N} e^{\frac{-x^2}{2(s\sigma)^2}} \tag{41}$$

to the original image, given the complementary scaling transformation (40) with its associated inverse mapping of the scale parameters $s \mapsto s^{-1}$. Since this is a family of rescaled and L_1 -normalised Gaussians, the scale channel network will compute a representation computationally equivalent to a Gaussian scale-space representation.

B Relation between scale channel networks and scale-normalised derivatives

We, here, describe the relationship between scale channel networks and scale-normalised derivatives. Assume that a

scale channel network in some layer learns a kernel that corresponds to a *Gaussian derivative*. We will show that when this kernel is applied to all the scale channels this correspond to a normalisation over scales of the kernels that is equivalent to applying scale-normalised derivatives at different scales in a scale-space representation of the original image.

B.1 Preliminaries: Gaussian derivatives in terms of Hermite polynomials

As a preparation for the intended result, we will first establish a relation between Gaussian derivatives and probabilistic Hermite polynomials. The probabilistic Hermite polynomials $He_n(x)$ are in 1-D defined by the relationship

$$He_n(x) = (-1)^n e^{x^2/2} \partial_{x^n} \left(e^{-x^2/2} \right) \tag{42}$$

implying that

$$\partial_{x^n} \left(e^{-x^2/2} \right) = (-1)^n He_n(x) e^{-x^2/2} \tag{43}$$

and

$$\partial_{x^n} \left(e^{-x^2/2\sigma^2} \right) = (-1)^n He_n\left(\frac{x}{\sigma}\right) e^{-x^2/2\sigma^2} \frac{1}{\sigma^n}. \tag{44}$$

Applied to a Gaussian function in 1-D, this implies that

$$\begin{aligned}
\partial_{x^n} (g(x; \sigma)) &= \\
&= \frac{1}{\sqrt{2\pi}\sigma} \partial_{x^n} \left(e^{-x^2/2\sigma^2} \right) \\
&= \frac{1}{\sqrt{2\pi}\sigma} \frac{(-1)^n}{\sigma^n} He_n\left(\frac{x}{\sigma}\right) e^{-x^2/2\sigma^2} \\
&= \frac{(-1)^n}{\sigma^n} He_n\left(\frac{x}{\sigma}\right) g(x; \sigma).
\end{aligned} \tag{45}$$

B.2 Scaling relationship for Gaussian derivative kernels

Let us assume that the scale channel network at some layer has learned a kernel that corresponds to a Gaussian partial derivative at some scale σ :

$$\begin{aligned}
\partial_{x^\alpha} g(x; \sigma) &= \\
&= \partial_{x_1^{\alpha_1} x_2^{\alpha_2} \dots x_N^{\alpha_N}} g(x; \sigma) = g_{x_1^{\alpha_1} x_2^{\alpha_2} \dots x_N^{\alpha_N}}(x; \sigma)
\end{aligned} \tag{46}$$

For later convenience, we write this learned kernel as a scale-normalised derivative at scale σ for $\gamma = 1$ multiplied by some constant C :

$$h(x) = C \sigma^{\alpha_1 + \alpha_2 + \dots + \alpha_N} g_{x_1^{\alpha_1} x_2^{\alpha_2} \dots x_N^{\alpha_N}}(x; \sigma). \tag{47}$$

Then, the corresponding family of equivalent kernels $h_s(x)$ in the dual representation (36), which represents the same effect on the original image as applying the kernel $h(x)$ to

a set of rescaled images $f_s(x) = f(x/s)$, provided that a complementary scaling transformation and the inverse mapping of the scale parameter $s \mapsto s^{-1}$ are performed, is given by

$$h_s(x) = \frac{1}{s^N} h\left(\frac{x}{s}\right) = \frac{C}{s^N} \sigma^{\alpha_1+\alpha_2+\dots+\alpha_N} g_{x_1^{\alpha_1} x_2^{\alpha_2} \dots x_N^{\alpha_N}}\left(\frac{x}{s}; \sigma\right). \quad (48)$$

Using Eq. (45) with

$$g(x; \sigma) = \frac{1}{(\sqrt{2\pi}\sigma)^N} e^{-(x_1^2+x_2^2+\dots+x_N^2)/2\sigma^2} \quad (49)$$

in N dimensions, we obtain

$$\begin{aligned} h_s(x) &= \frac{C}{s^N} \sigma^{\alpha_1+\alpha_2+\dots+\alpha_N} (-1)^{\alpha_1+\alpha_2+\dots+\alpha_N} \\ &\quad H e_{\alpha_1}\left(\frac{x_1}{s\sigma}\right) H e_{\alpha_2}\left(\frac{x_2}{s\sigma}\right) \dots H e_{\alpha_N}\left(\frac{x_N}{s\sigma}\right) \\ &\quad \frac{1}{(\sqrt{2\pi}\sigma)^N} e^{-(x_1^2+x_2^2+\dots+x_N^2)/2s^2\sigma^2} \frac{1}{\sigma^{\alpha_1+\alpha_2+\dots+\alpha_N}} \\ &= C(s\sigma)^{\alpha_1+\alpha_2+\dots+\alpha_N} (-1)^{\alpha_1+\alpha_2+\dots+\alpha_N} \\ &\quad H e_{\alpha_1}\left(\frac{x_1}{s\sigma}\right) H e_{\alpha_2}\left(\frac{x_2}{s\sigma}\right) \dots H e_{\alpha_N}\left(\frac{x_N}{s\sigma}\right) \\ &\quad \frac{1}{(\sqrt{2\pi}s\sigma)^N} e^{-(x_1^2+x_2^2+\dots+x_N^2)/2s^2\sigma^2} \frac{1}{(s\sigma)^{\alpha_1+\alpha_2+\dots+\alpha_N}}. \end{aligned} \quad (50)$$

Comparing with (45), we recognise this expression as the scale-normalised derivative

$$h_s(x) = C(s\sigma)^{\alpha_1+\alpha_2+\dots+\alpha_N} g_{x_1^{\alpha_1} x_2^{\alpha_2} \dots x_N^{\alpha_N}}(x; s\sigma) \quad (51)$$

of order $\alpha = (\alpha_1, \alpha_2, \dots, \alpha_N)$ at scale $s\sigma$.

This means that if the scale channel network learns a partial Gaussian derivative of some order, then the application of that filter to all the scale channels is computationally equivalent to *applying corresponding scale-normalised Gaussian derivatives* to the original image at all scales, given the complementary scaling transformation (40) with its associated inverse mapping of the scale parameters $s \mapsto s^{-1}$.

Specifically, this result implies that a scale channel network that combines the multiple scale channels by a max pooling operation over scales will have a similar function as scale selection performed by detecting global extrema of scale-normalised derivatives over scales, and thus share similarities to classical methods for scale selection [7, 8, 104].

While this result has been expressed for partial derivatives, a corresponding results holds also for derivative operators that correspond to directional derivatives of Gaussian kernels in arbitrary directions. This result can be easily understood from the expression for a directional derivative operator ∂_{e^n} of order $n = n_1 + n_2 + \dots + n_N$ in direction

$$\begin{aligned} e &= (e_1, e_2, \dots, e_N) \text{ with } |e| = \sqrt{e_1^2 + e_2^2 + \dots + e_N^2} = 1: \\ \partial_{e^n} g(x; \sigma) &= (e_1 \partial_{x_1} + e_2 \partial_{x_2} + \dots + e_N \partial_{x_N})^n g(x; \sigma) \\ &= \sum_{\alpha_1+\alpha_2+\dots+\alpha_N=n} \binom{n}{\alpha_1! \alpha_2! \dots \alpha_N!} \\ &\quad e_1^{\alpha_1} e_2^{\alpha_2} \dots e_N^{\alpha_N} \partial_{x_1}^{\alpha_1} \partial_{x_2}^{\alpha_2} \dots \partial_{x_N}^{\alpha_N} g(x; \sigma) \\ &= \sum_{\alpha_1+\alpha_2+\dots+\alpha_N=n} \binom{n}{\alpha_1! \alpha_2! \dots \alpha_N!} \\ &\quad e_1^{\alpha_1} e_2^{\alpha_2} \dots e_N^{\alpha_N} g_{x_1^{\alpha_1} x_2^{\alpha_2} \dots x_N^{\alpha_N}}(x; \sigma). \end{aligned} \quad (52)$$

Since the scale normalisation factors $\sigma^{|\alpha|}$ for all scale-normalised partial derivatives of the same order $|\alpha| = \alpha_1 + \alpha_2 + \dots + \alpha_N = n$ are the same, it follows that all linear combinations of partial derivatives of the same order are transformed by the same multiplicative scale normalisation factor, which proves the result.

C The MNIST Large Scale dataset

We, here, give a more detailed description of the *MNIST Large Scale dataset*. The original MNIST dataset [108] contains images of centered handwritten digits of size 28×28 . The MNIST Large Scale dataset is derived from the MNIST dataset by rescaling the original MNIST images. The resulting dataset contains images of size 112×112 with scale variations of a factor of 16. The scale factors s relative the original MNIST images are $s \in [\frac{1}{2}, 8]$. The dataset is illustrated in Figure 3.

To create an image with a certain scale factor s , the original image is first rescaled/resampled using bicubic interpolation. The image range is then clipped to $[0, 256]$ to remove possible over/undershoot resulting from the bicubic interpolation. The resulting image is embedded into an 112×112 resolution image using zero padding or cropping as needed.

Large amounts of upsampling tends to result in discretisation artefacts. To reduce the severity of such artefacts, the images are post-processed with discrete Gaussian smoothing [114] followed by non-linear thresholding. The standard deviation of the discrete Gaussian kernel varies with the scale factor as $\sigma(s) = \frac{7}{8}s$. After smoothing, the image range is rescaled to the range $[0, 255]$.

As a final step, an arctan non-linearity is applied to sharpen the resulting image, where the final image intensity I_{out} is computed from the output of the smoothing step I_{in} as:

$$I_{out} = \frac{2}{\pi} \arctan(a(I_{in} - b)) \quad (53)$$

with $a = 0.02$ and $b = 128$. Note that for scale factors > 4 , the full digit might not be visible in the image. These scale

factors are included to enable studying the limits of generalisation when the entire object is no longer visible (typically the digits are fully contained in the image for $s < 4\sqrt{2}$).

All training data sets are created from the first 50 000 images in the original MNIST training set, while the last 10 000 images in the original MNIST training set are used to create validation sets. The testing data sets are created by rescaling the 10 000 images in the original MNIST testing set. For the multi-scale datasets, scale factors for the individual images are sampled uniformly on a logarithmic scale in the range $[s_{min}, s_{max}]$.

The specific MNIST Large Scale dataset used for the experiments in this paper is available online [109].

References

1. Biederman, I., Cooper, E.E.: Size invariance in visual object priming. *Journal of Experimental Physiology: Human Perception and Performance* **18** (1992) 121–133
2. Logothetis, N.K., Pauls, J., Poggio, T.: Shape representation in the inferior temporal cortex of monkeys. *Current Biology* **5** (1995) 552–563
3. Ito, M., Tamura, H., Fujita, I., Tanaka, K.: Size and position invariance of neuronal responses in monkey inferotemporal cortex. *Journal of Neurophysiology* **73** (1995) 218–226
4. Furmanski, C.S., Engel, S.A.: Perceptual learning in object recognition: Object specificity and size invariance. *Vision Research* **40** (2000) 473–484
5. Hung, C.P., Kreiman, G., Poggio, T., DiCarlo, J.J.: Fast readout of object identity from macaque inferior temporal cortex. *Science* **310** (2005) 863–866
6. Isik, L., Meyers, E.M., Leibo, J.Z., Poggio, T.: The dynamics of invariant object recognition in the human visual system. *Journal of Neurophysiology* **111** (2013) 91–102
7. Lindeberg, T.: Feature detection with automatic scale selection. *International Journal of Computer Vision* **30** (1998) 77–116
8. Lindeberg, T.: Edge detection and ridge detection with automatic scale selection. *International Journal of Computer Vision* **30** (1998) 117–154
9. Lindeberg, T., Gårding, J.: Shape-adapted smoothing in estimation of 3-D shape cues from affine distortions of local 2-D structure. *Image and Vision Computing* **15** (1997) 415–434
10. Bretzner, L., Lindeberg, T.: Feature tracking with automatic selection of spatial scales. *Computer Vision and Image Understanding* **71** (1998) 385–392
11. Chomat, O., de Verdiere, V., Hall, D., Crowley, J.: Local scale selection for Gaussian based description techniques. In: Proc. European Conf. on Computer Vision (ECCV 2000). Volume 1842 of Springer LNCS., Dublin, Ireland (2000) I:117–133
12. Baumberg, A.: Reliable feature matching across widely separated views. In: Proc. Computer Vision and Pattern Recognition (CVPR'00). (2000) I:1774–1781
13. Mikolajczyk, K., Schmid, C.: Scale and affine invariant interest point detectors. *International Journal of Computer Vision* **60** (2004) 63–86
14. Lowe, D.G.: Distinctive image features from scale-invariant keypoints. *International Journal of Computer Vision* **60** (2004) 91–110
15. Bay, H., Ess, A., Tuytelaars, T., van Gool, L.: Speeded up robust features (SURF). *Computer Vision and Image Understanding* **110** (2008) 346–359
16. Tuytelaars, T., Mikolajczyk, K.: A Survey on Local Invariant Features. Volume 3(3) of Foundations and Trends in Computer Graphics and Vision. Now Publishers (2008)
17. Morel, J.M., Yu, G.: ASIFT: A new framework for fully affine invariant image comparison. *SIAM Journal of Imaging Sciences* **2** (2009) 438–469
18. Lindeberg, T.: Image matching using generalized scale-space interest points. *Journal of Mathematical Imaging and Vision* **52** (2015) 3–36
19. Lindeberg, T.: A computational theory of visual receptive fields. *Biological Cybernetics* **107** (2013) 589–635
20. Lindeberg, T.: Normative theory of visual receptive fields. *He- liyon* **7** (2021) e05897:1–20
21. Bruna, J., Mallat, S.: Invariant scattering convolution networks. *IEEE Trans. Pattern Analysis and Machine Intell.* **35** (2013) 1872–1886
22. Wu, F., Hu, P., Kong, D.: Flip-rotate-pooling convolution and split dropout on convolution neural networks for image classification. *arXiv preprint arXiv:1507.08754* (2015)
23. Marcos, D., Volpi, M., Tuia, D.: Learning rotation invariant convolutional filters for texture classification. In: International Conference on Pattern Recognition (ICPR 2016). (2016) 2012–2017
24. Cohen, T., M. Welling, M.: Group equivariant convolutional networks. In: International Conference on Machine Learning (ICML 2016). (2016) 2990–2999
25. Dieleman, S., Fauw, J.D., Kavukcuoglu, K.: Exploiting cyclic symmetry in convolutional neural networks. In: International Conference on Machine Learning (ICML 2016). (2016)
26. Laptev, D., Savinov, N., Buhmann, J.M., Pollefeys, M.: Ti-pooling: Transformation-invariant pooling for feature learning in convolutional neural networks. In: Proc. Computer Vision and Pattern Recognition (CVPR 2016). (2016) 289–297
27. Worrall, D.E., Garbin, S.J., Turmukhambetov, D., Brostow, G.J.: Harmonic networks: Deep translation and rotation equivariance. In: Proc. Computer Vision and Pattern Recognition (CVPR 2017). (2017) 5028–5037
28. Zhou, Y., Ye, Q., Qiu, Q., Jiao, J.: Oriented response networks. In: Proc. Computer Vision and Pattern Recognition (CVPR 2017). (2017) 519–528
29. Marcos, D., Volpi, M., Komodakis, N., Tuia, D.: Rotation equivariant vector field networks. In: Proc. International Conference on Computer Vision (ICCV 2017). (2017) 5048–5057
30. Cohen, T.S., Welling, M.: Steerable CNNs. In: International Conference on Learning Representations (ICLR 2017). (2017)
31. Weiler, M., Geiger, M., Welling, M., Boomsma, W., Cohen, T.: 3d steerable CNNs: Learning rotationally equivariant features in volumetric data. In: Advances in Neural Information Processing Systems (NIPS 2018). (2018) 10381–10392
32. Weiler, M., Hamprecht, F.A., Storath, M.: Learning steerable filters for rotation equivariant CNNs. In: Proc. Computer Vision and Pattern Recognition (CVPR 2018). (2018) 849–858
33. Worrall, D., Brostow, G.: Cubenet: Equivariance to 3D rotation and translation. In: Proc. European Conference on Computer Vision (ECCV 2018). Volume 11209 of Springer LNCS. (2018) 567–584
34. Cheng, G., Han, J., Zhou, P., Xu, D.: Learning rotation-invariant and Fisher discriminative convolutional neural networks for object detection. *IEEE Trans. Image Processing* **28** (2018) 265–278
35. Cohen, T.S., Geiger, M., Koehler, J., Welling, M.: Spherical CNNs. In: International Conference on Learning Representations (ICLR 2018). (2018)
36. Thomas, N., Smidt, T., Kearnes, S., Yang, L., Li, L., Kohlhoff, K., Riley, P.: Tensor field networks: Rotation-and translation-equivariant neural networks for 3D point clouds. *arXiv preprint arXiv:1802.08219* (2018)
37. Xu, Y., Xiao, T., Zhang, J., Yang, K., Zhang, Z.: Scale-invariant convolutional neural networks. *arXiv preprint arXiv:1411.6369* (2014)

38. Kanazawa, A., Sharma, A., Jacobs, D.W.: Locally scale-invariant convolutional neural networks. arXiv preprint arXiv:1412.5104 (2014)

39. Marcos, D., Kellenberger, B., Lobry, S., Tuia, D.: Scale equivariance in CNNs with vector fields. arXiv preprint arXiv:1807.11783 (2018)

40. Ghosh, R., Gupta, A.K.: Scale steerable filters for locally scale-invariant convolutional neural networks. arXiv preprint arXiv:1906.03861 (2019)

41. Worrall, D., Welling, M.: Deep scale-spaces: Equivariance over scale. In: Advances in Neural Information Processing Systems (NeurIPS 2019). (2019) 7366–7378

42. Esteves, C., Allen-Blanchette, C., Zhou, X., Daniilidis, K.: Polar transformer networks. In: International Conference on Learning Representations (ICLR 2018). (2018)

43. Sermanet, P., LeCun, Y.: Traffic sign recognition with multi-scale convolutional networks. In: International Joint Conference on Neural Networks (IJCNN 2011). (2011) 2809–2813

44. Cai, Z., Fan, Q., Feris, R.S., Vasconcelos, N.: A unified multi-scale deep convolutional neural network for fast object detection. In: Proc. European Conference on Computer Vision (ECCV 2016). Volume 9908 of Springer LNCS. (2016) 354–370

45. Jaderberg, M., Simonyan, K., Zisserman, A., Kavukcuoglu, K.: Spatial transformer networks. In: Proc. Neural Information Processing Systems (NIPS 2015). (2015) 2017–2025

46. Lin, C.H., Lucey, S.: Inverse compositional spatial transformer networks. In: Proc. Computer Vision and Pattern Recognition (CVPR 2017). (2017) 2568–2576

47. Henriques, J.F., Vedaldi, A.: Warped convolutions: Efficient invariance to spatial transformations. In: International Conference on Machine Learning. Volume 70. (2017) 1461–1469

48. Sermanet, P., Eigen, D., Zhang, X., Mathieu, M., Fergus, R., LeCun, Y.: OverFeat: Integrated recognition, localization and detection using convolutional networks. arXiv preprint arXiv:1312.6229 (2013)

49. Girshick, R.: Fast R-CNN. In: Proc. International Conference on Computer Vision (ICCV 2015). (2015) 1440–1448

50. Lin, T.Y., Dollár, P., Girshick, R., He, K., Hariharan, B., Belongie, S.: Feature pyramid networks for object detection. In: Proc. Computer Vision and Pattern Recognition (CVPR 2017). (2017)

51. Lin, T.Y., Goyal, P., Girshick, R., He, K., Dollár, P.: Focal loss for dense object detection. In: Proc. International Conference on Computer Vision (ICCV 2017). (2017) 2980–2988

52. He, K., Gkioxari, G., Dollár, P., Girshick, R.: Mask R-CNN. In: Proc. International Conference on Computer Vision (ICCV 2017). (2017) 2961–2969

53. Hu, P., Ramanan, D.: Finding tiny faces. In: Proc. Computer Vision and Pattern Recognition (CVPR 2017). (2017) 951–959

54. Szegedy, C., Zaremba, W., Sutskever, I., Bruna, J., Erhan, D., Goodfellow, I., Fergus, B.: Intriguing properties of neural networks. arXiv preprint arXiv:1312.6199 (2013)

55. Nguyen, A., Yosinski, J., Clune, J.: Deep neural networks are easily fooled: High confidence predictions for unrecognizable images. In: Proc. Computer Vision and Pattern Recognition (CVPR 2015). (2015) 427–436

56. Moosavi-Dezfooli, S.M., Fawzi, A., Frossard, P.: Deepfool: a simple and accurate method to fool deep neural networks. In: Proc. Conference on Computer Vision and Pattern Recognition (CVPR 2016). (2016) 2574–2582

57. Tanay, T., Griffin, L.: A boundary tilting perspective on the phenomenon of adversarial examples. arXiv preprint arXiv:1608.07690 (2016)

58. Su, J., Vargas, D.V., Kouichi, S.: One pixel attack for fooling deep neural networks. arXiv preprint arXiv:1710.08864 (2017)

59. Moosavi-Dezfooli, S.M., Fawzi, A., Fawzi, O., Frossard, P.: Universal adversarial perturbations. In: Proc. Computer Vision and Pattern Recognition (CVPR 2017). (2017)

60. Baker, N., Lu, H., Erlikhman, G., Kellman, P.J.: Deep convolutional networks do not classify based on global object shape. PLoS Computational Biology **14** (2018) e1006613

61. Engstrom, L., Tran, B., Tsipras, D., Schmidt, L., Madry, A.: A rotation and a translation suffice: Fooling CNNs with simple transformations. arXiv preprint arXiv:1712.02779 (2017)

62. Fawzi, A., Frossard, P.: Manitest: Are classifiers really invariant? In: British Machine Vision Conference (BMVC 2015). (2015)

63. Cireşan, D., Meier, U., Schmidhuber, J.: Multi-column deep neural networks for image classification. arXiv preprint arXiv:1202.2745 (2012)

64. Dieleman, S., Willett, K.W., Dambre, J.: Rotation-invariant convolutional neural networks for galaxy morphology prediction. Monthly Notices of the Royal Astronomical Society **450** (2015) 1441–1459

65. Iijima, T.: Basic theory on normalization of pattern (in case of typical one-dimensional pattern). Bulletin of the Electrotechnical Laboratory **26** (1962) 368–388 (in Japanese).

66. Witkin, A.P.: Scale-space filtering. In: Proc. 8th Int. Joint Conf. Art. Intell., Karlsruhe, Germany (1983) 1019–1022

67. Koenderink, J.J.: The structure of images. Biological Cybernetics **50** (1984) 363–370

68. Koenderink, J.J., van Doorn, A.J.: Generic neighborhood operators. IEEE Trans. Pattern Analysis and Machine Intell. **14** (1992) 597–605

69. Lindeberg, T.: Scale-Space Theory in Computer Vision. Springer (1993)

70. Lindeberg, T.: Scale-space theory: A basic tool for analysing structures at different scales. Journal of Applied Statistics **21** (1994) 225–270 Also available from <http://www.csc.kth.se/~tony/abstracts/Lin94-SI-abstract.html>.

71. Florack, L.M.J.: Image Structure. Series in Mathematical Imaging and Vision. Springer (1997)

72. Weickert, J., Ishikawa, S., Imita, A.: Linear scale-space has first been proposed in Japan. Journal of Mathematical Imaging and Vision **10** (1999) 237–252

73. ter Haar Romeny, B.: Front-End Vision and Multi-Scale Image Analysis. Springer (2003)

74. Duits, R., Florack, L., de Graaf, J., ter Haar Romeny, B.: On the axioms of scale space theory. Journal of Mathematical Imaging and Vision **22** (2004) 267–298

75. Lindeberg, T.: Generalized Gaussian scale-space axiomatics comprising linear scale-space, affine scale-space and spatio-temporal scale-space. Journal of Mathematical Imaging and Vision **40** (2011) 36–81

76. Farabet, C., Couprie, C., Najman, L., LeCun, Y.: Learning hierarchical features for scene labeling. IEEE Trans. Pattern Analysis and Machine Intell. **35** (2013) 1915–1929

77. van Noord, N., Postma, E.: Learning scale-variant and scale-invariant features for deep image classification. Pattern Recognition **61** (2017) 583–592

78. Jansson, Y., Lindeberg, T.: Exploring the ability of CNNs to generalise to previously unseen scales over wide scale ranges. In: International Conference on Pattern Recognition (ICPR 2020). (2021) 1181–1188

79. Barnard, E., Casasent, D.: Invariance and neural nets. IEEE Transactions on Neural Networks **2** (1991) 498–508

80. Simonyan, K., Zisserman, A.: Very deep convolutional networks for large-scale image recognition. In: International Conference on Learning Representations (ICLR 2015). (2015) arXiv preprint arXiv:1409.1556.

81. Engstrom, L., Tran, B., Tsipras, D., Schmidt, L., Madry, A.: Exploring the landscape of spatial robustness. In: International Conference on Machine Learning (ICML 2019). (2019) 1802–1811

82. Singh, B., Davis, L.S.: An analysis of scale invariance in object detection — SNIP. In: Proc. Computer Vision and Pattern Recognition (CVPR 2018). (2018) 3578–3587

83. Ren, S., He, K., Girshick, R., Zhang, X., Sun, J.: Object detection networks on convolutional feature maps. *IEEE Trans. Pattern Analysis and Machine Intell.* **39** (2016) 1476–1481

84. Nah, S., Kim, T.H., Lee, K.M.: Deep multi-scale convolutional neural network for dynamic scene deblurring. In: Proc. Computer Vision and Pattern Recognition (CVPR 2017). (2017) 3883–3891

85. Chen, L.C., Papandreou, G., Kokkinos, I., Murphy, K., Yuille, A.L.: DeepLab: Semantic image segmentation with deep convolutional nets, atrous convolution, and fully connected CRFs. *IEEE Trans. Pattern Analysis and Machine Intell.* **40** (2017) 834–848

86. Yu, F., Koltun, V.: Multi-scale context aggregation by dilated convolutions. In: Int. Conf. on Learning Representations (ICLR 2016). (2016)

87. Yu, F., Koltun, V., Funkhouser, T.: Dilated residual networks. In: Proc. Computer Vision and Pattern Recognition (CVPR 2017). (2017) 472–480

88. Mehta, S., Rastegari, M., Caspi, A., Shapiro, L., Hajishirzi, H.: ESPNet: Efficient spatial pyramid of dilated convolutions for semantic segmentation. In: Proc. European Conference on Computer Vision (ECCV 2018). (2018) 552–568

89. Yang, F., Choi, W., Lin, Y.: Exploit all the layers: Fast and accurate CNN object detector with scale dependent pooling and cascaded rejection classifiers. In: Proc. Computer Vision and Pattern Recognition (CVPR 2016). (2016) 2129–2137

90. Zhang, R., Tang, S., Zhang, Y., Li, J., Yan, S.: Scale-adaptive convolutions for scene parsing. In: Proc. International Conference on Computer Vision (ICCV 2017). (2017) 2031–2039

91. Wang, H., Kembhavi, A., Farhadi, A., Yuille, A.L., Rastegari, M.: ELASTIC: Improving CNNs with dynamic scaling policies. In: Proc. Computer Vision and Pattern Recognition (CVPR 2019). (2019) 2258–2267

92. Chen, Y., Fang, H., Xu, B., Yan, Z., Kalantidis, Y., Rohrbach, M., Yan, S., Feng, J.: Drop an octave: Reducing spatial redundancy in convolutional neural networks with octave convolution. In: Proc. International Conference on Computer Vision (ICCV 2019). (2019)

93. Sifre, L., Mallat, S.: Rotation, scaling and deformation invariant scattering for texture discrimination. In: Proc. Computer Vision and Pattern Recognition (CVPR 2013). (2013) 1233–1240

94. Lindeberg, T.: Provably scale-covariant continuous hierarchical networks based on scale-normalized differential expressions coupled in cascade. *Journal of Mathematical Imaging and Vision* **62** (2020) 120–148

95. Lindeberg, T.: Scale-covariant and scale-invariant Gaussian derivative networks. In: Proc. Scale Space and Variational Methods in Computer Vision (SSVM 2021). Volume 12679 of Springer LNCS. (2021) 3–14 Extended version in arXiv preprint arXiv:2011.14759.

96. Cheng, G., Zhou, P., Han, J.: Learning rotation-invariant convolutional neural networks for object detection in VHR optical remote sensing images. *IEEE Transactions on Geoscience and Remote Sensing* **54** (2016) 7405–7415

97. Wang, Q., Zheng, Y., Yang, G., Jin, W., Chen, X., Yin, Y.: Multiscale rotation-invariant convolutional neural networks for lung texture classification. *IEEE Journal of Biomedical and Health Informatics* **22** (2017) 184–195

98. Bekkers, E.J., Lafarge, M.W., Veta, M., Eppenhof, K.A.J., Pluim, J.P.W., Duits, R.: Roto-translation covariant convolutional networks for medical image analysis. In: International Conference on Medical Image Computing and Computer-Assisted Intervention MICCAI 2018). Volume 11070 of Springer LNCS. (2018) 440–448

99. Lafarge, M.W., Bekkers, E.J., Pluim, J.P., Duits, R., Veta, M.: Roto-translation equivariant convolutional networks: Application to histopathology image analysis. *Medical Image Analysis* **68** (2020) 101849

100. Andrearczyk, V., Depeursinge, A.: Rotational 3D texture classification using group equivariant CNNs. *arXiv preprint arXiv:1810.06889* (2018)

101. Poggio, T.A., Anselmi, F.: *Visual Cortex and Deep Networks: Learning Invariant Representations*. MIT Press (2016)

102. Kondor, R., Trivedi, S.: On the generalization of equivariance and convolution in neural networks to the action of compact groups. In: International Conference on Machine Learning (ICML 2018). (2018)

103. Lindeberg, T., Florack, L.: Foveal scale-space and linear increase of receptive field size as a function of eccentricity. report, ISRN KTH/NA/P--94/27--SE, Dept. of Numerical Analysis and Computer Science, KTH (1994) Available from <http://www.csc.kth.se/~tony/abstracts/CVAP166.html>.

104. Lindeberg, T.: Scale selection. In Ikeuchi, K., ed.: *Computer Vision*. Springer (2021) https://doi.org/10.1007/978-3-03243-2_242-1.

105. Li, Y., Tax, D.M.J., Loog, M.: Supervised scale-invariant segmentation (and detection). In: Proc. Scale Space and Variational Methods in Computer Vision (SSVM 2011). Volume 6667 of Springer LNCS., Ein Gedi, Israel, Springer (2012) 350–361

106. Loog, M., Li, Y., Tax, D.M.J.: Maximum membership scale selection. In: *Multiple Classifier Systems*. Volume 5519 of Springer LNCS. (2009) 468–477

107. Lindeberg, T.: Scale selection properties of generalized scale-space interest point detectors. *Journal of Mathematical Imaging and Vision* **46** (2013) 177–210

108. LeCun, Y., Bottou, L., Bengio, Y., Haffner, P.: Gradient-based learning applied to document recognition. *Proceedings of the IEEE* **86** (1998) 2278–2324

109. Jansson, Y., Lindeberg, T.: MNIST Large Scale dataset. Zenodo (2020) Available at: <https://www.zenodo.org/record/3820247>.

110. Jansson, Y., Lindeberg, T.: Exploring the ability of CNNs to generalise to previously unseen scales over wide scale ranges. *arXiv preprint arXiv:2004.01536* (2020)

111. Li, Y., Tax, D.M.J., Loog, M.: Scale selection for supervised image segmentation. *Image and Vision Computing* **30** (2012) 991–1003

112. Krizhevsky, A., Hinton, G.: Learning multiple layers of features from tiny images. Technical report, University of Toronto (2009)

113. Lindeberg, T.: Generalized axiomatic scale-space theory. In Hawkes, P., ed.: *Advances in Imaging and Electron Physics*. Volume 178. Elsevier (2013) 1–96

114. Lindeberg, T.: Scale-space for discrete signals. *IEEE Trans. Pattern Analysis and Machine Intell.* **12** (1990) 234–254